REPORT DOCUMENTATION PAGE

Form Approved
OMB No. 0704-0188

1. REPORT DATE *(DD-MM-YY)*	2. REPORT TYPE	3. DATES COVERED *(From – To)*
13-06-2006	Final	01 Aug 2005 – 30 Apr 2006

4. TITLE AND SUBTITLE
MHD FLOW CONTROL AND POWER GENERATION IN LOW-TEMPERATURE SUPERSONIC FLOWS

5a. CONTRACT NUMBERS
FA9550-05-C-0121

5b. GRANT NUMBER

5c. PROGRAM ELEMENT NUMBER

6. AUTHORS
Sivaram P. Gogineni, Ph.D. Igor V. Adamovich, Ph.D.

5d. PROJECT NUMBER

5e. TASK NUMBER

5f. WORK UNIT NUMBER

7. PERFORMING ORGANIZATION NAME(S) AND ADDRESS(ES)
Innovative Scientific Solutions, Inc.
2766 Indian Ripple Road
Dayton, OH 45440-3638

The Ohio State University
Dept. of Mechanical Eng.
Columbus, OH 43202

8. PERFORMING ORGANIZATION REPORT NUMBER
2121 Final

9. SPONSORING/MONITORING AGENCY NAME(S) AND ADDRESS(ES)
USAF, AFRL, Air Force Office of Scientific Research
AFOSR/NA (Attn: Dr. John Schmisseur)
875 North Randolph Street, Suite 325, Room 3112
Arlington, VA 22203

10. SPONSORING/MONITORING AGENCY ACRONYM(S)
AFOSR/NA

11. SPONSORING/MONITORING

AFRL-SR-AR-TR-06-0301

12. DISTRIBUTION/AVAILABILITY STATEMENT
Approved for public release; distribution unlimited.

13. SUPPLEMENTARY NOTES

14. ABSTRACT
Report developed under STTR contract for topic AF05-T016. Results of cold MHD flow deceleration and MHD power-generation experiments conducted at The Ohio State University are presented. MHD effect on the flow is detected from flow static-pressure measurements. The observed static-pressure change is due to the MHD interaction and not Joule heating of the flow in the crossed discharge. Comparison of experimental results with modeling calculations shows that the retarding Lorentz force increases the static-pressure rise produced by Joule heating of the flow, while the accelerating Lorentz force reduces the pressure rise. The experiments show that at the present conditions, the electric current in the MHD power-generation regime is very low, on the order of 1 mA. This is entirely due to the bottleneck effect of the discharge cathode layer at conditions where the MHD open voltage is significantly lower than the cathode-voltage fall. Modeling calculations demonstrate that (1) at the flow conductivities currently achieved in low-temperature MHD flows ($\sigma \sim 0.1$ mho/m), low open voltages reduce the MHD currents by more than two orders of magnitude, and (2) this effect cannot be circumvented by seeding the flow at feasible levels (~ 0.1%) or using electrodes with a high secondary-emission coefficient.

15. SUBJECT TERMS STTR Report, MHD Flow Control, MHD Power Generation, Low-Temperature Plasma, Supersonic Flow, Molecular-Tagging Velocimetry

16. SECURITY CLASSIFICATION OF			17. LIMITATION OF ABSTRACT:	18. NUMBER OF PAGE	19a. NAME OF RESPONSIBLE PERSON
a. REPORT	b. ABSTRACT	c. THIS PAGE			John Schmisseur, Ph.D.
Unclassified	Unclassified	Unclassified	SAR	32	19b. TELEPHONE NUMBER (703) 696-6962

Table of Contents

List of Figures

List of Figures

1. Introduction

The use of nonequilibrium (low-temperature) magnetohydrodynamics for supersonic flow control and power generation continues to attract considerable interest. Over the last few years, numerous theoretical system studies and modeling calculations in this field have been complemented by experimental results. In particular, experiments at Ohio State showed that retarding Lorentz force results in significant density fluctuation increase in a supersonic boundary layer [1,2] and core flow deceleration [3] in low-temperature M=3 nitrogen and air flows. In these experiments, ionization in cold supersonic flows (stagnation temperature T_0=300 K) was generated by transverse RF discharge [1] and by high voltage, short pulse duration, high pulse repetition rate discharge [2,3]. The repetitively pulsed discharge ionization technique has also been used at Princeton University to demonstrate feasibility of MHD power extraction from a cold M=3 air flow [4]. Finally, nonequilibrium MHD flow experiments at Wright-Patterson AFB showed that a near-surface glow discharge combined with the magnetic field can be used to control surface pressure on a model in a M=5 air flow [5].

Considerable effort has been made to demonstrate cold supersonic flow acceleration or deceleration by Lorentz force, with the main application being MHD flow control in hypersonic inlets [6]. Recent results demonstrate Lorentz force acceleration of a constricted discharge filament sustained near the test section wall in a cold M=3 air flow, up to velocities of 1.9 km/sec [7]. If the momentum of the accelerated filament is coupled to the flow due to collisions between the charged species and the neutral species, this would result in the boundary layer flow acceleration (the "snowplow" effect hypothesized in Ref. [7]). Indeed, 3-D compressible Navier-Stokes MHD modeling calculations [8] suggest that Lorentz force flow acceleration and deceleration may be detected at the flow conductivities realized at the conditions of the experiment of Ref. [2], both in the boundary layer and in the inviscid core flow. Specifically, for a M=2.6 nitrogen flow at a stagnation pressure of P=1/3 atm, electrical conductivity of σ=0.1 mho/m, magnetic field of B_z=1.5 T, transverse electric field of E_y=±300 V/cm, and the MHD section length of L=5 cm, these calculations predict Mach number change by up to $\Delta M \approx \pm 0.2$. This Mach number change corresponds to a relative static pressure change of $\Delta P/P \approx \pm 30\%$, which would be easily detectable in the experiment. Indeed, such static pressure change, dependent on the Lorentz force direction, has been recently measured in cold MHD flows [3].

During the operation of an MHD channel, Joule heat is inevitably generated in addition to the Lorentz force. The ratio of the Joule heat, $j_y E_y$, to the Lorentz force work, $j_y B_z u$, determines the MHD loading parameter, $K = E_y/B_z u$, where $j_y \sim \sigma E_y$ is the transverse current density and u is the flow velocity. Obviously, increasing the electric field at a given conductivity would increase the Lorentz force. However, this would be achieved at the penalty of also increasing the loading parameter, which would mean that a larger fraction of input electrical power would simply heat the gas, without imparting momentum to the flow. In nonequilibrium nitrogen and air plasmas sustained in supersonic flows, the detrimental effect of Joule heating can be significantly reduced due to the well known fact that a major fraction of the electric discharge power at these conditions, up to 98% [9], goes to vibrational excitation of nitrogen. Since the supersonic flow residence time in the MHD section is quite short, $\tau_{res} \sim L/u \sim 0.1$ m / 10^3 m/s ~ 100 μsec, while vibrational relaxation time of nitrogen at low temperature is $P\tau_{VT} \sim 1$ atm·sec [10], vibrational relaxation simply does not have time to occur. In air, vibrational relaxation of nitrogen in the presence of O atoms generated in the discharge is much faster, $P\tau_{VT} \sim 10$ atm·μsec · (n_O/N) [10], where n_O/N is the O atom mole fraction. However, because the O atom fraction in the discharge

is rather small, vibrational relaxation would still remain very slow. For this reason, the energy would remain locked in the nitrogen vibrational mode and Joule heating in the discharge would be greatly reduced. The effective MHD loading parameter at these conditions can be defined as follows,

$$K = \frac{\alpha \cdot j_y E_y}{j_y B_z u} = \frac{\alpha \cdot E_y}{B_z u} \quad , \tag{1}$$

where α is the discharge energy fraction going into Joule heating. This well known effect provided rationale for completely neglecting Joule heating in modeling calculations of Ref. [8], as a first approximation. However, this approach is oversimplified, since it is understood that in the actual low-temperature MHD experiments [2], Joule heating, although significantly reduced, still remained a factor affecting the results. If the Lorentz force interaction indeed results in significant momentum transfer from the charged species to the entire supersonic flow, the flow static pressure would decrease for both j and B vectors configurations producing an accelerating Lorentz force and increase for the other two configurations producing a retarding Lorentz force. On the other hand, if the electric discharge power at these conditions remains the same, Joule heating would result in the static pressure increase (i.e. Mach number reduction), which would be the same for all four of these cases. In case when both these factors, Lorentz force and Joule heating, generate comparable effects on the flow, the static pressure dependence on the Lorentz force direction should still be apparent.

Feasibility of electrical power generation in low-temperature MHD flows is another key technical issue. The main potential application of this technology is power generation on board of hypersonic vehicles, where the use of gas turbines for this purpose may be highly problematic because of high flow stagnation temperatures. At M=6, the incident flow stagnation temperature is T_0=1600-1800 K, which approaches maximum gas turbine operation temperature but is still too low to produce sufficient thermal ionization and flow conductivity. Therefore, MHD power generation at these conditions would require external ionization. So far, power generation experiments in low-temperature MHD flows ionized by high-voltage pulses [4] produced extremely low MHD currents, less than 1 mA. This is several orders of magnitude lower than MHD current estimates based on the flow conductivities measured at similar conditions, σ~0.1 mho/m [2,3]. Clearly, further work is necessary to determine feasibility and potential scalability of this method of on-board power generation.

The objectives of the present work are as follows:

1. ***Studies of the Lorentz force effect on the flow Mach number, determined from the static pressure measurements. Identification and quantification of the Lorentz force polarity effect on the flow static pressure.***

2. ***Measurements of MHD power generation in low-temperature flows ionized by nanosecond duration, high voltage pulses. The main effort is to increase the current measured without voltage applied to the transverse (MHD) electrodes by using higher ionizing pulse voltage and pulse repetition rate, and by seeding the flow with an easily ionizable species.***

3. ***Kinetic modeling of a crossed ionizing pulser / MHD sustainer discharge in the presence of magnetic field used in the present experiments. The modeling calculations provide insight into the discharge kinetics and identify approaches to increase the MHD power generation current.***

2. Experimental

The experiments have been conducted at the supersonic nonequilibrium plasma/MHD wind tunnel facility described in greater detail in Refs. [1,2]. Briefly, this facility generates stable and diffuse supersonic nonequilibrium plasmas flows at M=3-4 in a uniform magnetic field up to B=2 T, with run durations from tens of seconds to complete steady state. The schematic of the M=3 supersonic nozzle and an MHD test section is shown in Fig.1. An aerodynamically contoured M=3 supersonic nozzle made of transparent acrylic plastic is connected to a 2 cm x 4 cm rectangular cross section test section 12 cm long with an angle step diffuser. The nozzle / test section / diffuser assembly is attached to a vacuum system connected to a 1200 ft^3 dump tank pumped out by an Allis-Chalmers 1300 cfm rotary vane vacuum pump. The minimum pressure in the vacuum system sustained by the pump is 35-40 torr, which necessitates the use of a supersonic diffuser with the nozzle / test section operated at relatively low stagnation and static pressures (P_0=1/3-1 atm, P_{test}=7-20 torr). The nozzle assembly is equipped with pressure taps measuring plenum pressure as well as static pressures at the beginning and at the end of the test section. The nozzle throat dimensions are 20 mm x 9.5 mm, which gives a mass flow rate through the test section of $\dot{m}$=15 g/sec at P_0=1/3 atm.

Two rectangular electrode blocks 5 cm long are flush mounted in the side test section walls (see Fig. 1). Each electrode block, made of mica ceramic, incorporates a single copper plate electrode 35 mm wide, 45 mm long, and 3 mm thick. The electrode edges are rounded using a Rogowski profile [11] to achieve a more uniform electric field distribution between the electrodes. To accommodate the electrodes, recesses are machined in the ceramic blocks. This creates a 2 mm thick ceramic layer between each electrode and the flow in the test section. On the opposite sides, the electrodes are covered with 2 mm thick acrylic plates. The gaps between the copper electrodes, the ceramic blocks, and the cover acrylic plates are filled with a self-hardening dielectric compound to preclude electrode surface exposure to air and prevent corona formation near the high-voltage electrode surface. Figure 2 shows a photograph of the M=3 test section. Ionization in the test section is produced using a Chemical Physics Technologies (CPT) custom designed high-voltage (up to 20 kV peak), short pulse duration (~10-20 nsec), high repetition rate (up to 50 kHz) pulsed plasma generator. During the pulser operation, pulse voltage and current are measured using a Tektronix P6015A high voltage probe and a custom-made low-capacitance resistive current probe. Several series of measurements have been conducted using an FID Technology pulsed power supply which operates at a significantly higher pulse repetition rate, ν=100 kHz, peak voltage up to 40 kV, and 5 nsec pulse duration, recently purchased by the OSU Nonequilibrium Thermodynamics Group.

Transverse DC electrical current (sustainer current) in the supersonic flow ionized by the repetitively pulsed discharge is sustained by applying a DC field (up to 500 V/cm) to two 50 mm x 20 mm DC electrode blocks flush mounted in the top and bottom nozzle walls 4 cm apart, perpendicular both to the flow velocity and to the magnetic field direction, as shown in Fig. 1. The applied DC field, which is far too low to produce additional ionization in the flow, except in

the cathode layer, is needed to sustain transverse (MHD) current. The DC electrode blocks are made of boron nitride ceramic, with continuous copper electrodes 45 mm long each. The transverse DC field is applied using a DEL 2 kV / 3A power supply operated in a voltage stabilized mode, with a 0.5-1.0 kΩ ballast. Two inductors 1 mH each were placed in the DC circuit in series with both DC electrodes to attenuate high amplitude current pulses propagation into the DC circuit. Current in the DC sustainer circuit is measured using a Tektronix AM503S current probe.

The entire nozzle / test section / diffuser assembly was placed between the poles of a GMW water cooled electromagnet, as shown in Figs. 1, 2, and attached to a 4 foot long, 6 inch diameter PVC vacuum pipe connected to the vacuum system. To improve the pulsed discharge load impedance matching, the high voltage pulse magnetic compression unit was also mounted inside the magnet, above the test section (see Fig. 2), and short high voltage electrode cables (15 cm long) have been used. The magnet can generate a steady-state magnetic field up to B=3.5 T between two circular poles up to 25 cm in diameter. In the present experiments, for the distance between the 15 cm diameter poles of 6 cm, the magnetic field at maximum current through the magnet coils of 140 A is B=1.8 T. To preclude external magnetic field penetration into the pulse compression unit, it was placed inside a custom-made six-layer shell magnetic shield made of a high magnetic permeability material with the total wall thickness of 1/2". Multiple layers are necessary because of the magnetic flux saturation in the outermost shield layers in the strong external magnetic field. At the B=1.5 T field between the magnet poles, the field inside the magnetic shield was about 20-30 mT.

Flow temperature downstream of the MHD section was inferred from the nitrogen second positive system emission spectra measured using a Thor Labs 5 m long AFS fiber optic bundle with collimators on each end, and a Princeton Instruments Optical Multichannel Analyzer (OMA) with a 0.5 m monochromator, 1200 g/mm grating blazed at 700 nm, and an ICCD array camera. The collimators were positioned in front of an optical access window in the test section (see Fig. 1), and in front of the slit opening of the spectrometer, respectively. Fiber optic link calibration using a 1.3 mm diameter aperture light source showed the collimator signal collection region to be a cylinder 2-3 mm in diameter and approximately 50 mm long [12]. Therefore these measurements yielded emission spectra averaged along the line of sight passing through the center plane of the flow (see Fig. 1). Rotational temperature of the flow was inferred using a synthetic spectrum with the accurate nitrogen molecular constants [13], rotational like intensities [14], and the experimentally measured slit function of the spectrometer.

To increase the flow electrical conductivity, the flow upstream of the nozzle plenum could be seeded with an easily ionizable chemical (1-Pyrrolidinocyclopentene, $C_9H_{15}N$) with ionization potential of 7.1 eV [15]. For this, an auxiliary nitrogen flow passing through a heated stainless steel bubbler filled with liquid cyclopentene-pyrrolidine was mixed with the main flow. Saturated vapor pressure of cyclopentene is 0.11 torr at $T=25^0$ C and 15 torr at 100^0 C [16]. The seed fraction in the MHD test section was estimated from the partial pressure of the nitrogen-seed mixture in the test section plenum, 15-30 torr at the total pressure of 250 torr, which gives the seed fraction of about 25-50 ppm at $T=25^0$ C and 750-1500 ppm at $T=40^0$ C.

In the present experiments, both the magnet and the DC power supply were operated continuously. No breakdown was produced in the test section and no current was measured in the DC circuit until the high voltage pulse train was initiated. After the gas flow was started and test section pressure reached steady state, the pulser was turned on for 0.5-1.0 seconds. After the high voltage pulse train stopped, the discharge always extinguished. Time-dependent static pressure at

the end of the test section was monitored by a high accuracy Omega PX811-005GAV pressure transducer, at a sampling rate of 67 Hz (time resolution of 15 msec). The pressure tap used for these measurements is located in the side wall of the test section, 3 cm downstream of the DC electrodes, as shown in Figs. 1,2. The pressure transducer was placed at a distance of about 2 m from the test section, which was sufficient to nearly completely remove electromagnetic interference from the pulsed discharge. As in our previous work [1,2], static pressure was measured for both accelerating and decelerating Lorentz force directions. In both these cases, Lorentz force was generated by two different combinations of the transverse B field and the transverse DC electric field directions. Control runs in a cold supersonic flow without plasmas and in an ionized flow without DC electric field applied, i.e. when the time-averaged Lorentz force is zero, have also been conducted. The purpose of this approach was to isolate the MHD effect, which should depend on the Lorentz force direction, from the polarity-independent effect of Joule heat. The experiments were conducted in nitrogen, dry air, and room air.

3. Discharge Model

Two-dimensional, time-dependent kinetic model of a nonequilibrium electric discharge sustained by external ionization in presence of transverse DC electric field and transverse magnetic field incorporates equations for electron and ion densities in drift-diffusion approximation and Poisson equation for the electric field [17],

$$\begin{aligned}
&\frac{\partial n_+}{dt}+\frac{\partial \Gamma_{+,x}}{dx}+\frac{\partial \Gamma_{+,y}}{dy}=\alpha(E_p/N)\mu_e E_p/N+\alpha(E/N)|\Gamma_e|-\beta_{ei}n_+n_e \\
&\frac{\partial n_e}{dt}+\frac{\partial \Gamma_{e,x}}{dx}+\frac{\partial \Gamma_{e,y}}{dy}=\alpha(E_p/N)\mu_e E_p/N+\alpha(E/N)|\Gamma_e|-\beta_{ei}n_+n_e \qquad (2)\\
&\frac{\partial^2\varphi}{dx^2}+\frac{\partial^2\varphi}{dy^2}=-\frac{e}{\varepsilon_0}(n_+-n_e)
\end{aligned}$$

In Eqs. (2), n_+ and n_e are the ion and electron number densities, respectively, φ is the electric potential, α is the Townsend ionization coefficient by electron impact,

$$\alpha_{T=300\,K}=\begin{cases}900p(E/p)^{-1}\exp(-313p/E), & E/p<100\ V/(cm\cdot torr)\\ 12p\exp(-342p/E), & E/p\geq 100\ V/(cm\cdot torr)\end{cases} \qquad (3)$$

E_p is the electric field in a high-voltage ionizing pulse, $E=|\nabla\phi|$, N is the total number density, $\beta_{ei}=2\cdot10^{-7}$ cm^3/sec is the electron-ion recombination coefficient, and $\Gamma_{e,x}$, $\Gamma_{e,y}$, $\Gamma_{+,x}$, $\Gamma_{+,y}$ are the x- and y- components of electron and ion fluxes,

$$\Gamma_{+,x} = \frac{1}{1+\beta_+^2}\left(-D_+\frac{\partial n_+}{dx} + \mu_+ n_+ E_x\right) + \frac{\beta_+}{1+\beta_+^2}\left(-D_+\frac{\partial n_+}{dy} + \mu_+ n_+ E_y\right)$$

$$\Gamma_{+,y} = \frac{1}{1+\beta_+^2}\left(-D_+\frac{\partial n_+}{dy} + \mu_+ n_+ E_y\right) - \frac{\beta_+}{1+\beta_+^2}\left(-D_+\frac{\partial n_+}{dx} + \mu_+ n_+ E_x\right)$$

$$\Gamma_{e,x} = \frac{1}{1+\beta_e^2}\left(-D_e\frac{\partial n_e}{dx} - \mu_e n_e E_x\right) - \frac{\beta_e}{1+\beta_e^2}\left(-D_e\frac{\partial n_e}{dy} - \mu_e n_e E_y\right) \quad (4)$$

$$\Gamma_{e,y} = \frac{1}{1+\beta_e^2}\left(-D_e\frac{\partial n_e}{dy} - \mu_e n_e E_y\right) + \frac{\beta_e}{1+\beta_e^2}\left(-D_e\frac{\partial n_e}{dx} - \mu_e n_e E_x\right)$$

$$|\Gamma_e| = \sqrt{\Gamma_{e,x}^2 + \Gamma_{e,y}^2} \quad (5)$$

In Eqs. (4), β_e and β_+ are the electron and ion Hall parameters, and μ_e and μ_+ are the mobilities, and D_e and D_+ are the diffusion coefficients,

$$\beta_+ = \mu_+ B_z,\ \beta_e = \mu_e B_z$$

$$\mu_+ = \frac{1.45\times10^3}{p}\frac{cm^2}{V\cdot s},\ \mu_e = \frac{4.4\times10^5}{p}\frac{cm^2}{V\cdot s} \quad (6)$$

$$D_+ = \mu_+\frac{k_B T}{e},\ D_e = \mu_e\frac{k_B T_e}{e}$$

The pressure and temperature of the gas in the discharge were assumed to be P=7 torr and T=110 K. The electron temperature was estimated to be T_e=1 eV. The time dependence of ionizing pulsed electric field was assumed to be Gaussian,

$$E_p(t) = \frac{U_p}{w}\exp\left[-\left(\frac{t-t_0}{\tau}\right)^2\right], \quad (7)$$

where U_p is the peak voltage, w=2 cm is distance between the pulsed electrodes (test section width), and τ=15 nsec is the pulse width. Since the model does not calculate the voltage fall in the pulsed electrode sheaths, which could be as high as several kV [18], parameter U_p was adjusted to correctly predict the experimentally measured current voltage characteristics of the sustainer discharge (i.e. plasma conductivity), U_p=2.7 kV. The spatial distribution of the pulsed electric field, $E_p(x,y)$, was calculated from the Rogowski profile of the pulser electrode edges.

Boundary conditions on the cathode (at y=0), at the anode (at y=1), and away from the ionization region (at x=0,1) are as follows:

$$
\begin{aligned}
&y = 0 \\
&\frac{\partial n_+}{dy} = 0,\ n_e = \gamma n_+ \frac{\mu_+}{\mu_e},\ \ \varphi = 0 \\
&y = 1 \\
&n_+ = 0,\ \ \frac{\partial n_e}{dy} = 0,\ \ \varphi = V \\
&x = 0, 1 \\
&\frac{\partial n_+}{dx} = \frac{\partial n_e}{dx} = \frac{\partial \varphi}{dx} = 0
\end{aligned}
\tag{8}
$$

System of equations (2) was solved using a stiff partial differential equation solver PDETWO [19].

4. Results and Discussion

4.1. Flow acceleration (loading parameter K>1)

Figure 3 shows typical single pulse voltage and current oscillograms in a M=3 nitrogen flow at P_0=250 torr, P_{test}=8.4 torr, respectively, at the magnetic field of B=1.5 T. The peak voltage and current at these conditions are 13.2 kV and 31.2 A, respectively, with pulse duration (FWHM) of approximately 30 ns. The pulse energy coupled to the flow, calculated from the current and voltage traces at these conditions, was in the range of 1-2 mJ.

Figure 4 shows several voltage pulses generated at the pulse repetition rate of ν= 40 kHz, at the same flow conditions. From Fig. 4, it can be seen that at this pulse repetition rate the voltage duty cycle is extremely low, ~30 nsec / 25 μsec ~ 1/1000. The high reduced electric field during the pulses, E/N~$70 \cdot 10^{-16}$ V·cm^2 (700 Td), makes possible efficient ionization by electron impact, the rates of which have strong exponential dependence on E/N [9]. On the other hand, the short pulse duration and the low duty cycle greatly improve the plasma stability. Basically, the pulse duration, ~30 nsec, is much shorter than the characteristic time for the ionization instability development, ~10^{-3}-10^{-4} sec [9].

Figure 5 shows DC sustainer current oscillograms in a pulse-ionized M=3 nitrogen flow at the conditions of Figs. 3 and 4. In Fig. 5, current traces are shown for DC power supply voltage of U_{PS}=2 kV and ballast resistor of R=0.5 kΩ, for two different electric field polarities. Since the DC power supply operates in the voltage stabilized mode, the voltage between the DC electrodes is $U=U_{PS}-IR$, where I is the sustainer current. In this figure, the current pulses produced during the high voltage pulses are not resolved. It can be seen that after each ionizing pulse the sustainer current reaches approximately I=2 A, with the subsequent fall-off in a decaying plasma between the pulses, to a minimum value of about I=0.5 A. Note that the plasma does not fully decay between the pulses. As can be seen from Fig. 5, the time-averaged currents at these conditions are close, <I>=0.95 and 0.86 A. In dry air at the same flow and plasma conditions, the time average currents were up to <I>=1.0-1.3 A. In the entire range of

experimental conditions, the discharge plasma appeared uniform and stable, filling the entire volume of the flow in the MHD section. Magnetic field helped stabilizing the discharge, dissipating sustainer current oscillations occurring in the absence of the magnetic field. Photographs of the pulser-sustainer plasmas generated in supersonic flows of nitrogen and air can be found in our recent paper [2]. This behavior suggests that the supersonic plasma flow in the MHD section can be analyzed using a quasi-one-dimensional MHD flow model.

The time-averaged DC discharge power added to the flow at these conditions is approximately 1.1-1.5 kW. Instant thermalization at a mass flow rate of $\dot{m}$=15 g/sec would result in the estimated flow temperature rise of about ΔT=70-100 K, from the baseline core flow temperature at M=2.9 of T=110 K. However, at the reduced electric field in the sustainer discharge of $E/N=(5\text{-}6)\cdot 10^{-16}$ V·cm^2 (based on the initial core flow temperature), about 90% of the discharge power in nitrogen and air goes to vibrational excitation of nitrogen [9], vibrational relaxation rate of which is extremely slow [10]. Basically, the slow vibrational relaxation rate locks up the energy stored in nitrogen vibrations and makes the supersonic flow essentially frozen. Assuming that the rest of the discharge power (~10%) thermalizes, the resultant inviscid core flow temperature rise would be significantly lower, only up to ~10 K. Note that energy addition to the flow by the repetitively pulsed discharge, based on the measured single pulse energy, 1-2 mJ, is insignificant, 40-80 W at the pulse repetition rate of ν=40 kHz, or only a few per cent of the energy loading by the DC sustainer discharge.

These estimates are consistent with the flow temperature measurements. Figure 6 shows two $N_2(C^3\Pi_u \rightarrow B^3\Pi_g)$ emission spectra (rotationally unresolved 1→4 band) measured in a M=3 nitrogen flow ionized by a repetitively pulsed discharge at ν=40 kHz and B=1.5 T, (i) without the DC sustainer discharge and (ii) at the highest sustainer discharge power of 1.4 kW, achieved at U_{PS}=2 kV, R=0.5 kΩ, and $\langle I \rangle$=0.9 A. Note that these spectra are very nearly identical, although the line-of-sight averaging by the fiber optic collimator includes signal contribution from the boundary layers flowing over the DC electrode surfaces (see Fig. 1), where heating by DC discharge is likely to be most intense. The best fit synthetic spectrum, shown in Fig. 7, indicates the line-of-sight averaged temperature of T=180±20 K for both these cases (i.e. ~40-80 W power added by the pulser alone and ~1.5 kW added by pulser and sustainer together). This temperature is somewhat higher than the isentropic flow temperature at M=2.9, T=110 K. This is most likely due to the line-of sight averaging across the core flow and two boundary layers on the top and bottom walls of the test section (see Fig. 1). Contribution of warm boundary layer regions (with the recovery temperature of T_r=270 K) into the spectrum results in raising the "tail" of the vibrational band, thereby increasing the apparent rotational temperature. This effect has also been observed in our previous work on shock wave control in M=2 low-temperature RF plasma flows [20]. We emphasize that the most important result is that the temperatures measured with and without the DC sustainer discharge turn out to be very close. Note that instant thermalization of the DC sustainer discharge power at these conditions would result to a flow temperature rise of approximately ΔT=90 K. Figure 7, which shows N_2 synthetic spectra at T=100, 180, and 260 K, illustrates the sensitivity of the temperature inference method used, and demonstrates that a temperature rise of 90 K would be easily detected at the present spectral resolution. Therefore, absence of a detectable temperature rise produced by a 1.4 kW DC sustainer discharge is direct evidence of delayed flow thermalization due to slow vibrational relaxation.

Figure 8 shows normalized test section static pressure traces measured in M=3 nitrogen flows at the conditions of Figs. 3-5, with and without Lorentz force applied. The baseline static pressure, measured using the pressure tap downstream of the MHD section shown in Figs. 1, 2,

was P=8.4 torr, which corresponds to the Mach number of M=2.9. Turning the pulser on in the presence of magnetic filed, without applying transverse DC electric field, i.e. generating ionization in the test section without applying Lorentz force did not produce detectable pressure rise (see Fig. 8). This suggests that Joule heating generated by the pulser is negligibly small. In addition to this baseline pressure trace, four pressure traces plotted in Fig. 8 correspond to four possible combinations of the transverse current and the magnetic field vector directions, shown schematically in Fig. 1. Two of these combinations result in accelerating Lorenz force, **jxB**, while two others produce retarding Lorentz force. In each one of these runs, the pulser was turned on for 0.5 sec.

From Fig. 8, it can be seen that in all four cases, generating transverse current in the MHD section results in the static pressure increase. This behavior points to Joule heating of the flow by the transverse DC discharge as one of the sources of the pressure rise. However, for both **j** and **B** vector combinations corresponding to the accelerating Lorentz force the pressure rise, 5-7%, is noticeably lower than for both retarding Lorentz force combinations, 18-21%. The dependence of the static pressure rise on the Lorentz force polarity suggests that the pressure and the flow Mach number may also be affected by the MHD force interaction. Similar results were obtained in a dry air flow at the same flow conditions (see Fig. 9), 5-7% for the accelerating Lorentz force and 17-20% for the retarding Lorentz force.

Control runs in nitrogen and dry air have been made with the magnetic field turned off, at B=0. In the absence of the magnetic filed, sustainer discharge voltage had to be reduced to U_{PS}=1 kV to prevent sustainer current oscillations and instability development. As a result, the discharge power decreased from about 1.5 kW (see Fig. 5) to about 0.5 kW. The sustainer current at these conditions, <I>=0.60-0.65 A, was comparable to the current at B=1.5 T, <I>=0.86-0.95 A (see Fig. 5). In this case, no pressure difference was detected between two DC discharge polarities, the pressure rise being about 3% in both cases (see Fig. 10). This provides additional evidence that the static pressure difference detected at B=1.5 T and shown in Figs. 8,9 is indeed due to the Lorentz force interaction.

To analyze the results of static pressure measurements in the presence of the Lorentz force and Joule heat, we have used quasi-one-dimensional MHD flow equations [21],

$$\frac{dp}{dx} = \frac{1}{M^2-1}\cdot\left[-\left\{(\gamma-1)M^2+1\right\}\cdot F + \frac{(\gamma-1)M}{a}\cdot\dot{Q}\right] \tag{9}$$

$$\frac{dM}{dx} = \frac{1}{ap}\cdot\frac{1}{M^2-1}\cdot\left\{u\left(1+\frac{\gamma-1}{2}M^2\right)\cdot F - \frac{\gamma-1}{2\gamma}\cdot\left(\gamma M^2+1\right)\cdot\dot{Q}\right\} \tag{10}$$

$$\frac{du}{dx} = \frac{u}{p}\cdot\frac{1}{M^2-1}\cdot\left(F - \frac{\gamma-1}{\gamma u}\cdot\dot{Q}\right) \tag{11}$$

$$\frac{dT}{dx} = \frac{T}{p}\cdot\frac{\gamma-1}{\gamma}\cdot\frac{1}{M^2-1}\cdot\left(-\gamma M^2\cdot F + \frac{\gamma M^2-1}{u}\cdot\dot{Q}\right) \quad , \tag{12}$$

where

$$F = j_y B_z \cong \frac{IB}{A} \tag{13}$$

$$\dot{Q} = \alpha \cdot j_y E_y \cong \alpha \cdot \frac{I(U_{PS} - IR)}{Ah} \tag{14}$$

are the Lorentz force and the Joule heat per unit volume, respectively. In Eqs. (13,14), I is the sustainer current, U_{PS} is the DC voltage, R is the ballast resistance, A is the DC electrode surface area, h is the distance between the DC electrodes, and α is the discharge power fraction going to Joule heating (effective Joule heating factor). Note that for small values of the MHD interaction parameter [21],

$$\eta = \frac{\left| j_y B_z \right| L}{\rho u_\infty^2} \quad , \tag{15}$$

the right hand sides of Eqs. (9-12) are nearly constant, and they can be integrated analytically. In Eq. (15), L is the length of the MHD section. Indeed, at the conditions of the present experiments, U_{PS}=2 kV, $I_y \approx$1.0 A, R=0.5 kΩ, B=1.5 T, A=9 cm^2, L=4.5 cm, $\rho \approx 0.03$ kg/m^3, and $u_\infty \approx 600$ m/sec, the interaction parameter is quite low, $\eta \approx 7 \cdot 10^{-3}$. Then integrating Eq. (9) gives the following expressions for the pressure rise difference between the retarding and the accelerating Lorentz force cases, $\Delta p_R - \Delta p_A$,

$$\Delta p_R - \Delta p_A \cong 2 \cdot \frac{(\gamma - 1)M^2 + 1}{M^2 - 1} \cdot j_y B_z L \tag{16}$$

and for the effective Joule heating factor,

$$\alpha \cong \frac{\Delta p_A + \Delta p_R}{2} \frac{M^2 - 1}{(\gamma - 1)M} \frac{a}{j_y E_y L} \tag{17}$$

For the baseline conditions, p=8.5 torr, T=110 K, M=2.9, γ=1.4, Eq. (16) gives $(\Delta p_R - \Delta p_A)/p \approx 0.08$ for I=1 A. Note that the estimated pressure difference is consistent with the experimental results for nitrogen and air shown in Figs. 8,9. Using Eq. (17) with the results of Fig. 8, the effective Joule heating factor is $\alpha \approx 0.11 \pm 0.015$. The effective Joule heating factor inferred from the static pressure rise measurements is in good agreement with the results of Bolzmann equation solution [22], α=0.09 in nitrogen at the reduced electric field of $E/N = 6 \cdot 10^{-16}$ V·cm^2 and α=0.10 in air at $E/N = 5 \cdot 10^{-16}$ V·cm^2. At these conditions, the effective MHD loading parameter (the ratio of the Joule heating and the Lorentz force work), given by Eq. (1), is $K \approx 4$. Therefore, this analysis suggests that the observed static pressure difference between the accelerating and the retarding Lorentz force runs is indeed due to the MHD force interaction, superimposed on the pressure rise due to Joule heating of the flow in the discharge.

The rate of the flow velocity change due to MHD interaction, predicted by Eq. (11), can be also estimated from simple analysis of momentum transfer from the charged particles (electrons and ions) to the neutrals by collisions. Indeed, the Lorentz force applied to the plasma as a whole is balanced by the collision drag force,

$$e(n_e\mu_e + n_i\mu_i)E_y B_z = (n_e m_e \nu_{en} + n_i m_i \nu_{in})(u_p - u) \tag{18}$$

Note that the Coulomb forces on the electrons and the ions produced by the Hall (polarization) field cancel out. In Eq. (18), n_e and n_i are electron and ion number densities, respectively, m_e and m_i are their masses, μ_e and μ_i are their mobilities, ν_{en} and ν_{in} are electron-neutral and ion-neutral collision frequencies, and u_p-u is the plasma velocity relative to the flow (ion slip velocity [23]). Assuming that charge separation in the plasma due to the Hall effect is small, so that $n_e \approx n_i$, and using $\mu_e = e/m_e\nu_{en}$ and $\mu_i = e/m_i\nu_{in}$, we have

$$e(\mu_e + \mu_i)E_y B_z = \left(\frac{1}{\mu_e} + \frac{1}{\mu_i}\right)(u_p - u) \tag{19}$$

Finally, remembering that $\mu_e >> \mu_i$, the ion slip velocity is

$$u_p - u \approx \mu_e \mu_i E_y B_z \tag{20}$$

Equation (20), also obtained in Ref. [24], is in good agreement with recent measurements of the ion slip velocity (near-surface constricted discharge filament velocity) in a weakly ionized low-temperature M=3 flow at B=2 T [7]. Since the neutral velocity changes in an ion-neutral collision and in a electron-neutral collision are $\sim(u_p\text{-}u)$ and $\sim(m_e/m_i)(u_p\text{-}u) << (u_p\text{-}u)$, respectively, the net rate of the neutral flow velocity change is

$$\frac{du}{dt} \approx \nu_{in}\frac{n_e}{N}(u_p - u) = \frac{j_y B_z}{\rho} = \frac{F}{\rho} \tag{21}$$

Finally, remembering that $\rho = \gamma p M^2/u^2$, we obtain

$$\frac{du}{dx} \approx \frac{u}{P}\frac{F}{\gamma M^2} \tag{22}$$

which at $M^2 >> 1$ and in the absence of Joule heat is consistent with Eq. (11). This simple estimate, along with the ion slip velocity measurements [7], demonstrates that phenomenological MHD flow equations, Eqs. (9-12), are consistent with the plasma behavior on the microscopic level.

To estimate the effect of the rate of vibrational relaxation of nitrogen on the effective Joule heating factor, α, one series of experiments was done in room air. In this case, two additional factors change the sustainer discharge characteristics considerably. First, energy added to the vibrational mode of nitrogen by the sustainer discharge thermalizes more rapidly due to

fast vibrational relaxation of nitrogen on water vapor, $P\tau_{VT} \sim 10$ atm·μsec at room temperature [25]. Second, electrons in the plasma rapidly attach to oxygen in three-body collisions with water molecules,

$$e + O_2 + H_2O \rightarrow O_2^- + H_2O \quad , \tag{23}$$

with a near gas kinetic rate, $k=1.4\cdot10^{-29}$ cm^6/s [9]. The latter effect is clearly evident in Fig. 11, which shows sustainer discharge currents in M=3 dry air and room air flows at the same conditions, P_0=250 torr, P_{test}=8.7 torr, B=1.5 T, U_{PS}=2 kV, and R=1.0 kΩ. It can be seen that adding water vapor reduces the current decay time (plasma life time) by about an order of magnitude, from about 25 μsec to about 2-3 μsec. Because of this, the time-averaged current in Fig. 11 also drops by a factor of ten, from <I>=0.51 A to <I>=0.052 A, which suggests that the Lorentz force effect in room air flows would be negligibly small. Indeed, Fig. 12 shows essentially no difference in static pressures rise for the accelerating and retarding Lorentz force directions in room air flows at these conditions. However, from Fig. 12 it can be seen that the static pressure rise due to Joule heating in room air, 6±2%, is comparable to the pressure rise in dry air at the same flow conditions (see Fig. 9), in spite of an order of magnitude difference in the sustainer discharge current and power. Using Eq. (17) with the results of Fig. 12 gives an estimate of the effective Joule heating factor in room air, α=0.4±0.15. This result shows that adding water vapor substantially accelerates the rate of Joule heating in supersonic nonequilibrium plasma flows, most likely due to accelerated vibrational relaxation of nitrogen.

The characteristic time for the flow static pressure change due to both MHD forcing and Joule heating of the supersonic core flow should be comparable with the flow residence time in the discharge section, ~100 μsec. However, the pressure rise/fall time measured in the present experiments is much longer, ~0.2 sec (see Figs. 8-10, 12), which is about an order of magnitude longer than the time resolution of the data acquisition system used, about 15 msec. Clearly, the measured rise/fall time is affected by an additional factor. Varying the length of the ¼" diameter plastic line connecting the wall static pressure tap and the pressure transducer showed that it is in fact the long line that controls the pressure measurement system response time. Indeed, Fig. 13 shows the normalized static pressure signals measured at the same conditions, in a M=3 nitrogen flow with a retarding Lorentz force applied, for two different line lengths, 1.9 m and 4.4 m. It can be seen that increasing the line length also increased the signal response time from about 0.2 sec to about 0.5 sec, without changing the steady-state pressure value. In the present experiments, removing the line and placing the pressure transducer near the static pressure tap was not feasible because of strong electromagnetic interference of the pulsed discharge with the transducer.

Figure 14 compares static pressure measurements with the results of numerical integration of Eqs. (9-12), for three different values of the effective Joule heating parameter, α=0 (no Joule heating), α=0.05, and α=0.10. Experimental points in Fig. 14 are obtained by measuring the static pressure 0.2 seconds after turning the pulser on, approximately at the moment when the pressure reached near steady state. In Fig. 14, positive values of the current correspond to the accelerating Lorentz force. It can be seen that the results of calculations for α=0.10 are in good agreement with the experimental data. Figure 14 also illustrates how Joule heating superimposed over Lorentz force affects the static pressure change. Specifically, while the calculations at α=0 (no Joule heating) predict static pressure reduction (i.e. Mach number increase) for the accelerating MHD force and static pressure increase (i.e. Mach number reduction) for the retarding MHD force, Joule heating results in static pressure rise in both cases.

However, the predicted static pressure increase is always higher for the retarding MHD force, which was observed in the present experiments.

Figure 15 plots the calculated flow Mach number at the conditions of Fig. 14. Comparing the results shown in Fig. 14 and Fig. 15 at α=0.10, it can be seen that at I=1.0 A flipping the Lorentz force direction from accelerating to retarding results in a Mach number change from M=2.77 to 2.64 (ΔM=-0.13). Since the baseline Mach number is M=2.89, it is apparent that in both these cases the combined effect of Lorentz force and Joule heating results in flow deceleration. However, as expected, flow deceleration is more pronounced for the retarding Lorentz force. From Fig. 15, one can also see that in the absence of Joule heating the Mach number change at I=1.0 A would be from M=2.96 to M=2.83 (at the same baseline Mach number of M=2.89), ΔM=-0.13. This Mach number change is lower than predicted by the 3-D compressible MHD Navier-Stokes calculations [8], ΔM=-0.4 at the baseline Mach number of M=2.6. However, in these calculations the MHD current was assumed to be I=3 A, which is approximately a factor of three higher than has been achieved in the present experiments. Raising transverse current in the quasi-one-dimensional model of Eqs. (9-12) up to I=3 A results in the increase of the Mach number change, ΔM=-0.42, which is very close to the result obtained in Ref. [8].

Figure 16 summarizes the results for the normalized static pressure difference for two Lorentz force directions, $(\Delta p_R - \Delta p_A)/p$, as a function of the transverse sustainer current obtained in M=3 nitrogen and dry air flows. It can be seen that the measured relative pressure change increases nearly proportional to the current and reaches about 13% at <I>=1.2-1.3 A. This behavior is in good agreement with the quasi-1-D MHD theory, both an approximate analytic solution, Eq. (16), and numerical integration of coupled Eqs. (9-12).

We conclude that the dependence of the static pressure change on the Lorentz force magnitude and polarity, which is consistent with the results of the quasi-one-dimensional MHD flow analysis, conclusively demonstrates supersonic flow deceleration by the Lorentz force. We emphasize that this effect could be detected only because the Joule heating factor in nitrogen and in dry air is small, α=0.1. If this were not the case, at low electrical conductivities achieved at the present experimental conditions the MHD effect would be overshadowed by Joule heating of the flow. To the best of our knowledge, this is the first time this effect was experimentally demonstrated in cold supersonic gas flows. This result, however, does not yet demonstrate feasibility of large-scale MHD deceleration of supersonic flows, discussed in Ref. [6]. This would require analysis of other critical technical issues, such as sustaining magnetic field and low energy cost external ionization over large volumes of the flow, as well as boundary layer separation in a decelerating flow.

Demonstration of net MHD acceleration of the flow, when the Mach number increase and the static pressure is reduced, would require reducing Joule heating, $\dot{Q}$, while keeping the Lorentz force, F, the same. From Eqs. (16,17), it can be seen that this is equivalent to reducing the loading parameter, determined by Eq. (1), to K~1. Since at the present experimental conditions the loading parameter is K~4 (at α=0.1), this suggests that net flow acceleration could be achieved if either the effective Joule heating factor or transverse electric field are reduced by a factor of four, down to α=0.025 or E_y=100 V/cm, respectively, or if the magnetic field is increased by a factor of four, up to B=6 T. Note that keeping the Lorentz force the same while reducing the electric field can be done only if the effective electrical conductivity of the flow, σ, is increased, so that the same transverse current, $j_y \sim \sigma E_y$, would be sustained at a lower transverse electric field. Therefore reducing the electric field by a factor of four would require quadrupling

the conductivity. We believe that the use of a new high-power FID pulsed plasma generator, with the pulse repetition rate of up to 100 kHz (2.5 times higher than the CPT pulser used in the flow acceleration experiments so far), peak voltage of up to 40 kV (2 times higher than the CPT pulser), and pulse duration of about 5 nsec (a factor of 5 shorter than the CPT pulser) would result in a very significant conductivity increase, which would be sufficient for demonstration of true M=3 flow acceleration. This will constitute a major thrust of the Phase II proposal.

4.1. Power Generation (Loading Parameter K<1)

Figure 17 shows current voltage characteristics of the MHD sustainer discharge in M=3 nitrogen flows at P_0=250 torr and P_{test}=7.5 torr [2]. It can be seen that at low voltages the sustainer current remains very low and nearly independent of the applied voltage, while at high voltages the current exhibits linear voltage dependence, as expected for the constant conductivity plasma. Basically, if the applied DC voltage is low, the voltage across the cathode layer of the discharge (cathode voltage fall) is insufficient to produce multiplication of secondary electrons emitted from the cathode surface and sustain a significant current, even at the conditions when the conductivity in the positive column of the discharge is high. For this, a well-known cathode layer self-sustaining criterion [9] must be satisfied,

$$\alpha d = \ln(1 + 1/\gamma) \tag{24}$$

In Eq. (24), α is the Townsend ionization coefficient by the DC sustainer field, given by Eq. (3), d is the cathode layer thickness, and γ is the secondary emission coefficient. Similar results have been obtained for dry air [2]. The cathode falls for different B fields are determined from the x-axis intercept of the linear slope of the current voltage characteristics. At the absence of magnetic field, the cathode fall in nitrogen is U_c=260±50 V, which is close to the normal self-sustained glow discharge cathode fall, U_c=208 V for copper cathode [9]. The cathode fall increases with the magnetic field, up to U_c=500±50 V B=1.5 T (see Fig. 17). This result is consistent with the electrical breakdown theory in crossed electric and magnetic fields, which predicts cathode layer self-sustaining voltage to increase with the magnetic field because of the Hall effect [26],

$$U_c = \frac{C \cdot Nd\sqrt{1+\beta^2}}{\ln\left(Nd\sqrt{1+\beta^2}\right) + \ln\left(\dfrac{A}{\ln(1+1/\gamma)}\right)} \tag{25}$$

In Eq. (25), N in the number density, β is the Hall parameter, and A and C are constants in the expression for the Townsend ionization coefficient in the crossed E and B fields,

$$\frac{\alpha}{N} = A\sqrt{1+\beta^2} \cdot \exp\left(-\frac{C\sqrt{1+\beta^2}}{E/N}\right) \tag{26}$$

Equation (25) is in good agreement with measurements of breakdown voltages in crossed fields in nitrogen [27]. The electrical conductivity of the flow and the Hall parameter were found from the slopes of the current voltage characteristics using Ohm's law [21]

$$I = \frac{\sigma}{\sqrt{1+\beta^2}}(U - U_c)\frac{A}{h} \tag{27}$$

σ=0.073 mho/m, β=1.2±0.12 at B=0.75 T and β=1.8±0.35 at B=1.5 T. In Eq. (27), σ is the scalar electric conductivity, A=9 cm^2 is the total surface area of the DC electrodes, and h=4 cm is the test section height.

Figure 18 shows MHD open voltages measured between DC electrodes disconnected from the load at B=±1.5 T, at the same flow conditions as in Fig. 17. It can be seen that the open voltages are U_{open}=25-30 V, which is consistent with the theoretical value, U_{open}=uBh=36 V, and much smaller than the cathode fall at these conditions, U_c=500±50 V (compare with Fig. 17). Since the open voltage is the highest possible potential difference between the MHD electrodes in the power generation regime (at the loading parameter K=1), this suggests that the MHD power generation current produced at the present experimental conditions would be very low, of the order of a few mA (see Fig. 17). Indeed, sustainer current measurements in pulse-ionized M=3 nitrogen flows at DC voltages of 100-500 V showed sharp current drop as the voltage was reduced, from 170 mA to about 8 mA (see Fig. 19). Note that the series of measurements shown in Figs. 19-21 was conducted at a significantly higher pulse repetition rate, ν=100 kHz, using a new 40 kV peak voltage, 5 nsec pulse duration FID pulsed power supply. MHD current was also measured in the power generation regime, when MHD electrodes were connected through a 500 Ohm load resistor and no DC voltage was applied. In this case, the time averaged current was approximately 1 mA. However, no detectable difference was measured between the MHD currents for two magnetic field directions, B=±1.5 T (see Fig. 20), which suggests that the measured current may have been affected by the residual ionizing pulse current (peaking at 30 A, see Fig. 3) leaking into the DC circuit rather than induced by the Lorentz force. This result, which is a direct consequence of the MHD open voltage being nearly an order of magnitude lower than the cathode fall, is consistent with Faraday current measurements in a crossed pulser-sustainer discharge in a M=3 supersonic air flow at B=5 T and low DC voltages [4], I=0.5-1.0 mA.

First experiments in seeded nitrogen flows showed that seeding the flow with room temperature $C_9H_{15}N$ vapor at a ~100 ppm level (at the bubbler temperature of 25^0 C) actually reduces the conductivity. Figure 21 shows sustainer currents measured in nitrogen and in N_2-$C_9H_{15}N$ flow ionized by a pulsed discharge at the same pulse repetition rate, 100 kHz, and DC voltage, 500 V. It can be seen that adding seed to the flow results in the sustainer current reduction by approximately a factor of two. At first, this result appears counterintuitive since ionization energy of $C_9H_{15}N$, 7.1 eV, is about half of that of N_2, 15 eV. However, condensation of the seed vapor in the low-temperature supersonic test section and liquid droplet formation may result in charge accumulation in the droplets, which would produce a significant reduction in charge mobility and electrical conductivity. To reduce this effect, the bubbler with liquid $C_9H_{15}N$ was moved closer to the test section (from 20 ft away to 3 ft away), and heated up to 40^0 C. This resulted in flow conductivity increase up to the unseeded nitrogen level (see Fig. 21). However, further experiments in seeded N_2 flows have not resulted in conductivity increase above the

unseeded flow level. We believe that the seed vapor condensation in the cold supersonic flow and charged droplet formation in the MHD test section remains a major effect affecting floe conductivity.

4.2. Discharge Modeling Calculations

The discharge model described in Section 3 was used to model the pulser-sustainer discharge in a magnetic field, operating at the present experimental conditions. Figure 22 shows comparison of the experimental and calculated sustainer discharge current voltage characteristics at B=0. It can be seen that the model correctly predicts the sustainer current behavior as a function of the applied DC voltage, including the cathode voltage fall of approximately U_c=300 V and a nearly linear slope at $U>U_c$, indicating electrical conductivity of σ=0.074 mho/m (time-averaged electron density of $n_e=2\cdot10^{11}$ cm^3/sec). This validation suggests that the model has predictive capability and can be used as a design tool for an in-depth analysis of the crossed MHD discharge characteristics.

Figure 23 summarizes the discharge parameters at B=0, U_{DC}=50 V (i.e. comparable with the open voltages measured in the present experiments), and $n_e=2\cdot10^{11}$ cm^3/sec. From Fig. 23, it can be seen that the electron density distribution in the discharge follows the ionizing electric field distribution between two rectangular pulser electrodes. Also, one can see that the DC sustainer electric field does not penetrate into the ionized region and remains confined to the charge separation (cathode layer) region. However, due to extremely slow secondary electron multiplication in the cathode layer at this low voltage, the electric current remains very low, I=0.52 mA. Specifically, the current to the cathode is due to the ion current produced by an electric field in that region, while the current to the anode is due to the electron diffusion current in a near absence of electric field. Both these currents are very low. We emphasize that the low current is entirely due to the bottleneck effect of the cathode layer. Indeed, without this effect at the present conditions, i.e. at the plasma conductivity of σ=0.074 mho/m, voltage of U_{DC}=50 V, and the DC electrode surface area of A=9 cm^2, the sustainer current would be I=83 mA.

To reduce the cathode layer effect, secondary emission coefficient was varied from the baseline value of γ=0.01 to γ=1.0, which comparable with the values measured for Be/Cu and Al_2O_3/Mo cathodes [28,29]. Townsend ionization coefficient, α, was also varied by adding up to 1000 ppm of $C_9H_{15}N$ to the mixture, assuming that parameter C for the seed in Eqs. (3, 26) is half that of nitrogen (an estimated value suggested by the ratio of ionization potential for $C_9H_{15}N$ and N_2, 7.1 eV and 15 eV), and that

$$\alpha = \alpha_{N_2}(1 - y_{seed}) + \alpha_{seed}\, y_{seed} \quad , \tag{28}$$

where $y_{seed}=10^{-3}$ is the seed mole fraction. These parametric calculations have resulted in a fairly weak change of the sustainer current (within about 50%). The main reason for this is that the effect of seed on the net ionization coefficient remains low because of the low seed fraction (see Eq. (28)), so the cathode layer self-sustaining criterion, Eq. (24), is still not satisfied. Also, the overall conductivity increases by less than 1%, which explains why adding the seed to the nitrogen flow have not resulted in detectable flow conductivity increase in MHD power generation experiments.

Figure 24 summarizes the discharge parameters at the same conditions as in Fig. 23 but in the presence of a B=1.5 T magnetic field. Again, it can be seen that the electron density follows the ionizing electric field distribution between two pulser electrodes, and that the sustainer electric field does not penetrate into the ionized region. In this case, the current circles over the periphery of the ionized region due to Lorentz force applied to moving electrons (see Fig. 24), but net current to the electrodes remains low, I=0.26 mA, which is again due to the bottleneck effect of the cathode layer. In this case, parametric calculations at different values of α and γ also did not show noticeable sustainer current increase. These parametric studies demonstrate that (i) at the flow conductivities currently achieved in low-temperature MHD flows, σ~0.1 mho/m, low open voltages reduce MHD currents by more than two orders of magnitude, and (ii) this effect cannot be circumvented by seeding the flow at feasible levels (~0.1%) or by using electrodes with high secondary emission coefficient (γ~1).

Based on the results of the present experiments and modeling calculations, the only feasible approach to extracting MHD power at these conditions is increasing the open voltage, U_{open}=uBL, from the present value of U_{open}=25-30 V to the value comparable with the cathode voltage fall at B=1.5 T, U_c=500±50 V. This can be achieved by increasing the flow velocity, magnetic field, or the MHD electrode separation L (i.e. scaling the size of flow ionization region). Note that in laboratory experiments using low stagnation temperature flows, the flow velocity cannot be significantly increased from the present value of u=600 m/sec. Also, increasing magnetic field above the presently used value of B=1.5 T would raise both the open voltage and the cathode voltage fall (e.g. see Fig. 17 and Eq. (25)), which makes this approach not very promising. The only remaining option is to significantly increase both the size of the pulsed ionized region and the MHD electrode separation (up to L=20-30 cm), while operating the MHD generator in the Hall mode [21, 23]. In this case, the MHD open voltage would be considerably higher, U_{open}=βuBL. Increase of the ionized region size and the MHD electrode separation could be achieved by using the fast ionization wave technique recently developed in Russia [30,31], and by using disk MHD generator ideally suited for operation in the Hall mode [32]. For this, we are planning to use a new high-power FID pulser recently purchased by our group. This will also constitute a major thrust of the Phase II proposal.

5. Summary

The report presents results of cold MHD flow deceleration and MHD power generation experiments using repetitively pulsed, short pulse duration, high voltage discharge to produce ionization in M=3 nitrogen and air flows in the presence of transverse DC electric field and transverse magnetic field.

MHD effect on the flow is detected from the flow static pressure measurements. Retarding Lorentz force applied to the flow produces a static pressure increase of up to 17-20%, while accelerating force of the same magnitude applied to the same flow results in static pressure increase of up to 5-7%. The effect is produced for two possible combinations of the magnetic field and transverse current directions producing the same Lorentz force direction (both for accelerating and retarding force). This demonstrates that the observed static pressure change is indeed due to the MHD interaction, and not due to Joule heating of the flow in the crossed discharge. No discharge polarity effect on the static pressure was detected in the absence of the magnetic field. The measured static pressure changes are compared with modeling calculations

using quasi-one-dimensional MHD flow equations. The fraction of the discharge input power going into Joule heat in nitrogen and dry air, α=0.1, has been inferred from the present experiments, and used as one of the input parameters in the MHD flow model. This fraction is low, primarily because most of the discharge power remains frozen in the vibrational energy mode of nitrogen, and increases to α=0.4±0.15 in room air because of rapid nitrogen relaxation on water vapor. Comparison of the experimental results with the modeling calculations shows that the retarding Lorentz force increases the static pressure rise produced by Joule heating of the flow in the discharge, while the accelerating Lorentz force reduces the pressure rise. This result provides first direct evidence of cold supersonic flow deceleration by Lorentz force. Demonstration of MHD flow acceleration (flow Mach number increase due to accelerating Lorentz force) will constitute a major thrust of the Phase II proposal.

The experiments showed that at the present conditions (flow conductivity of σ=0.074 mho/m), electric current produced in the MHD power generation regime is very low, of the order of 1 mA. Analysis of current-voltage characteristics of the pulser-sustainer MHD discharge showed this to be entirely due to the bottleneck effect of the discharge cathode layer, at the conditions when the MHD open voltage is significantly lower than the cathode voltage fall. Basically, at low DC voltages, the voltage across the cathode layer of the discharge is insufficient to produce multiplication of secondary electrons emitted from the cathode surface and sustain a significant current, even at the conditions when the conductivity in the positive column of the discharge is high. Adding an easily ionizable species to the flow ($C_9H_{15}N$ at 0.1% level) did not result in the flow conductivity increase, primarily because of seed condensation and charged droplet formation in the cold supersonic flow. Kinetic modeling calculations of the pulser-sustainer MHD discharge have been used to study the bottleneck effect of the cathode layer on the MHD current at low applied voltages. Modeling calculations demonstrate that (i) at the flow conductivities currently achieved in low-temperature MHD flows, σ~0.1 mho/m, low open voltages reduce MHD currents by more than two orders of magnitude, and (ii) this effect cannot be circumvented by seeding the flow at feasible levels (~0.1%) or by using electrodes with high secondary emission coefficient (γ~1). Based on the results of the present experiments and modeling calculations, the only feasible approach to extracting MHD power at low flow temperatures is to increase the MHD open voltage to the value comparable with the discharge cathode voltage fall. In the laboratory experiments, this can be achieved only by increasing the size of the pulsed ionized region and the MHD electrode separation (up to L=20-30 cm), while operating the MHD generator in the Hall mode. This will be a major thrust of the Phase II proposal.

6. References

1. R. Meyer, M. Nishihara, A. Hicks, N. Chintala, M. Cundy, W.R. Lempert, I.V. Adamovich, and S. Gogineni, "Measurements of Flow Conductivity and Density Fluctuations in Supersonic Nonequilibrium MHD Flows", AIAA Journal, Vol. 43, No. 9, 2005, pp. 1923-1930
2. M. Nishihara, N. Jiang, J.W. Rich, W.R. Lempert, I.V. Adamovich, and S. Gogineni, "Low-Temperature Supersonic Boundary Layer Control Using Repetitively Pulsed MHD Forcing", Physics of Fluids, Vol. 17, No. 10, 2005, pp. 106102-106102-12

3. M. Nishihara, J.W. Rich, W.R. Lempert, and I.V. Adamovich, "Low-Temperature M=3 Flow Deceleration by Lorentz Force", AIAA Paper 2006-1004, 44th Aerospace Sciences Meeting and Exhibit, January 2006, Reno, NV
4. R.C. Murray, S.H. Zaidi, M.R. Carraro, L.M. Vasilyak, S.O. Macheret, M.N. Shneider, and R.B. Miles, "Magnetohydrodynamic Power Generation Using Externally Ionized, Cold, Supersonic Air as Working Fluid", AIAA Journal, Vol. 44, No. 1, 2006, pp. 119-127
5. J. S. Shang, R. Kimmel, J. Hayes, C. Tyler and J. Menart, "Hypersonic Experimental Facility for Magnetoaerodynamic Interactions", Journal of Spacecraft and Rockets, Vol. 42, No. 5, 2005, pp. 780-789
6. A.L. Kuranov and E.G. Sheikin, "Magnetohydrodynamic Control on Hypersonic Aircraft under "Ajax" Concept", Journal of Spacecraft and Rockets, Vol. 40, No. 2, 2003, pp. 174-182
7. S. Zaidi, T. Smith, S. Macheret, and R. Miles, "Snowplow Surface Discharge in Magnetic Field for High Speed Boundary Layer Control", AIAA Paper 2006-1006, 44th AIAA Aerospace Sciences Meeting and Exhibit, Reno, NV, January 9-12, 2006
8. P. Rawat, X. Zhong, V. Singh, and S. Gogineni, "Numerical Simulation of Secondary Flow in a Weakly Ionized Supersonic Flow with Applied Electromagnetic Field", AIAA Paper 2005-5050, 36th AIAA Plasmadynamics and Lasers Conference, Toronto, Ontario, June 6-9, 2005
9. Yu. P. Raizer, "Gas Discharge Physics", Springer-Verlag, Berlin, 1991
10. B. F. Gordiets, V. A. Osipov, and L. A. Shelepin, "Kinetic Processes in Gases and Molecular Lasers", Gordon and Breach, London, 1988
11. J. D. Cobine, "Gaseous Conductors: Theory and Engineering Applications", Dover Publications, New York, 1958
12. S. Norberg, "Singlet Oxygen Generation in a High Pressure Non-Self-Sustained Electric Discharge", M.S. Thesis, Department of Mechanical Engineering, The Ohio State University, 2005
13. F. Roux, F. Michaud, and M. Vervloet, "High Resolution Fourier Spectrometry of $^{14}N_2$ Violet Emission Spectrum: Extensive Analysis of the $C3\Pi_u$-$B^3\Pi_g$ System", Journal of Molecular Spectroscopy, Vol. 158, 1993, pp. 270-277
14. A. Budo, " Intensitatsformeln fur die Triplettbanden", Zeitschrift fur Physik, Vol. 105, 1937, pp. 570-587
15. L.N. Domelsmith and K.N. Houk, "Photoelectron Spectra of Cyclopentanone and Cyclohexanone Enamines," Tetrahedron Letters, Vol 18, No. 23, 1977, pp. 1981-1984
16. http://ull.chemistry.uakron.edu/erd/
17. S.T. Surzhikov and J.S. Shang, "Two-Component Plasma Model for Two-Dimensional Glow Discharge in Magnetic Field", Journal of Computational Physics, Vol. 199, 2004, pp. 437-464
18. S.O. Macheret, M.N. Shneider, and R.C. Murray, "Ionization in Strong Electric Fields and Dynamics of Nanosecond-Pulsed Plasmas", Physics of Plasmas, Vol. 13, 2006, pp. 023502-023502-12
19. N.K. Madsen and R.F. Sincovec, ACM Transactions on Mathematical Software, Vol. 5, 1979, p. 326
20. S. Merriman, E. Plönjes, P. Palm, and I.V. Adamovich "Shock Wave Control by Nonequilibrium Plasmas in Cold Supersonic Gas Flows", AIAA Journal, Vol. 39, No. 8, 2001, pp. 1547-1552

21. G. W. Sutton and A. Sherman, "Engineering Magnetohydrodynamics", McGraw-Hill, New York, 1965
22. I. V. Adamovich, J. W. Rich, and G. L. Nelson, "Feasibility Study of Magneto-hydrodynamics Acceleration of Unseeded and Seeded Air Flows," AIAA Journal, Vol. 36, 1990, p. 590
23. R. J. Rosa, "Magnetohydrodynamic Energy Conversion", McGraw-Hill, 1968
24. S.O. Macheret, "Physics of Magnetically Accelerated Nonequilibrium Surface Discharges in High-Speed Flow", AIAA Paper 2006-1005, 44th AIAA Aerospace Sciences Meeting and Exhibit, Reno, Nevada, Jan. 9-12, 2006
25. H.E. Bass, S.D. Hoffman, H.-J. Bauer, "Laser Induced Fluorescence Study of the Deactivation of N_2^* by H_2O, H_2S, and CH_4", J. Chem. Phys., Vol. 72, No. 3, 1980, pp. 2113-2119
26. A. E. D. Heylen, "Electrical Ionization and Breakdown of Gases in a Crossed Magnetic Field," IEE Proceedings, Vol. 127, Pt. A, 1980, p. 221
27. C. L. Dargan and A. E. D. Heylen, "Uniform-Field Sparking Voltages of Gases in Crossed Magnetic Fields," Proceedings of IEE, Vol. 115, 1968, p. 1034
28. L. Laurenson and J.W. Koch, "The Secondary Electron Emission Characteristics of Clean and Contaminated Copper Beryllium Sheet", British Journal of Applied Physics, Vol. 16, 1965, pp. 889-892
29. J.J. Rocca, J.D. Meyer, M.R. Farrell, and G.J. Collins, "Glow-Discharge-Created Electron Beams: Cathode Materials, Electron Gun Designs, and Technological Applications", Journal of Applied Physics, Vol. 56, 1984, pp. 790-797
30. S.M. Starikovskaia, A.Yu. Starikovskii, and D.V. Zatsepin "Hydrogen Oxidation in a Stoichiometric Hydrogen-Air Mixtures in the Fast Ionization Wave", Combust. Theory Modeling, Vol. 5, 2001, pp. 97-129
31. S.M. Starikovskaia, N.B. Anikin, S.V. Pancheshnyi, D.V. Zatsepin, and A.Yu. Starikovskii, "Pulsed Breakdown at High Overvoltage: Development, Propagation and Energy Branching", Plasma Sources Sci. Technol., Vol. 10, 2001, p. 344
32. T. Fujino, Y. Watanabe, Y. Okuno, and H. Yamasaki, "The Effect of an Externally Applied Radio-Frequency Electromagnetic Field on the Performance of a Disk MHD Generator", Electrical Engineering in Japan, Vol. 140, 2002, pp. 789-794

7. Publications from Phase-I STTR Effort

M. Nishihara, J. W. Rich, W. R. Lempert, and I. V. Adamovich, "Low-Temperature M=3 Flow Deceleration by Lorentz Force," AIAA Paper 2006-1004, 44th Aerospace Sciences Meeting and Exhibit, January 2006, Reno, NV.

M. Nishihara, J. W. Rich, W. R. Lempert, I. V. Adamovich, and S. Gogineni, "Low-Temperature M=3 Flow Deceleration by Lorentz Force," submitted to Physics of Fluids; currently under review.

M. Nishihara, J. W. Rich, W. R. Lempert, I. V. Adamovich, and S. Gogineni "MHD Flow Control and Power Generation in Low-Temperature Supersonic Flows," AIAA Paper 2006-3076, 37th AIAA Plasmadynamics and Lasers Conference, June 2006, San Francisco, CA.

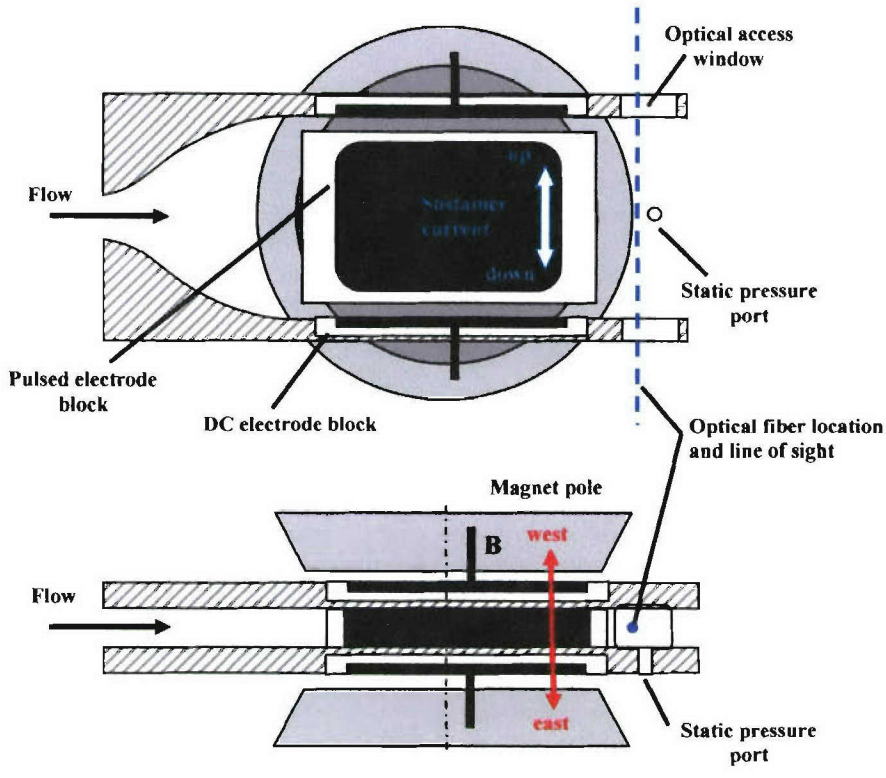

Figure 1. Schematic of a supersonic nozzle and MHD test section.

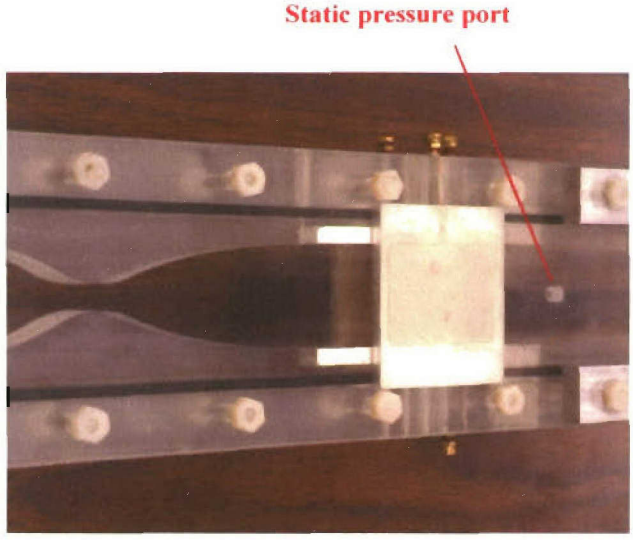

Figure 2. Photograph of a M=3 test section.

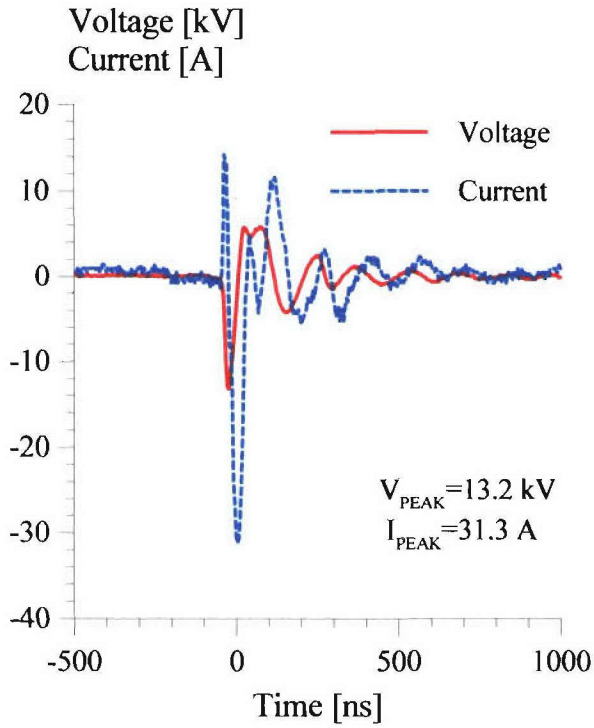

Figure 3. Single-pulse voltage and current oscillograms in M=3 nitrogen flow at P_0=250 torr, P_{test}=8.4 torr, and B=1.5 T.

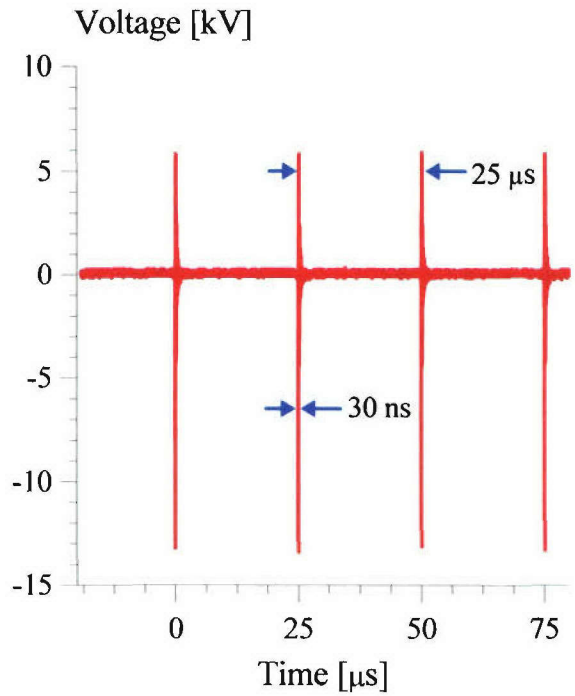

Figure 4. Repetitively pulsed voltage oscillogram in M=3 nitrogen flow at P_0=250 torr, P_{test}=8.4 torr, and B=1.5 T. Pulse repetition rate is ν=40 kHz.

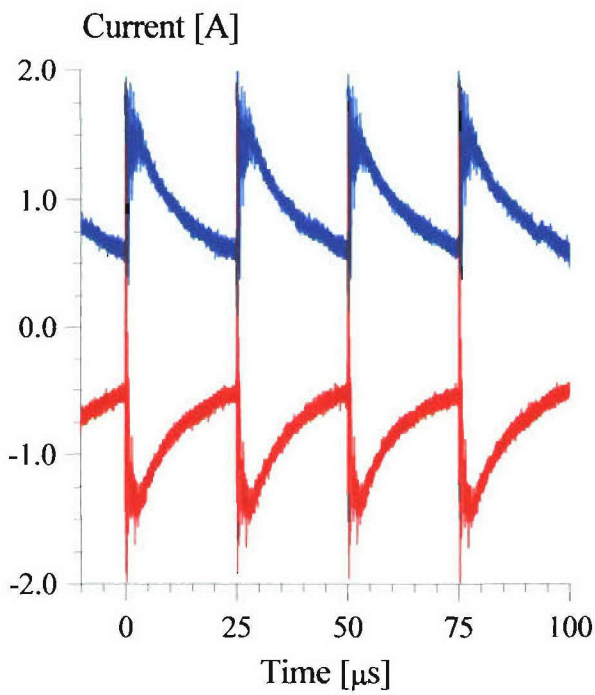

Figure 5. Sustainer (Faraday) current traces for two different transverse DC electric field polarities, at the conditions of Fig. 4. U_{PS}=2 kV, R=0.5 kΩ. Time-averaged currents are 0.95 A (top curve) and 0.86 A (bottom curve).

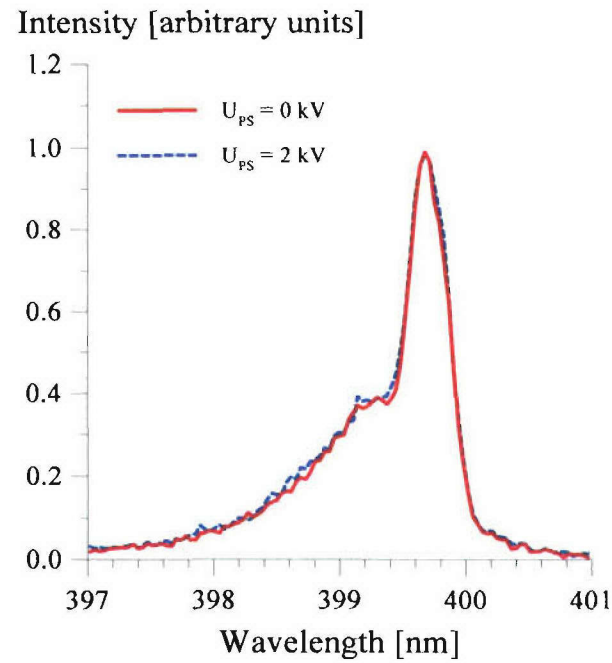

Figure 6. $N_2(C^3\Pi_u \rightarrow B^3\Pi_g)$ emission spectra (1→4 band) in M=3 nitrogen flow at P_0=250 torr, B=1.5 T, and ν=40 kHz, with and without 1.4 kW DC sustainer discharge. Synthetic spectrum fit indicates rotational temperature of T=180±20 K in both cases.

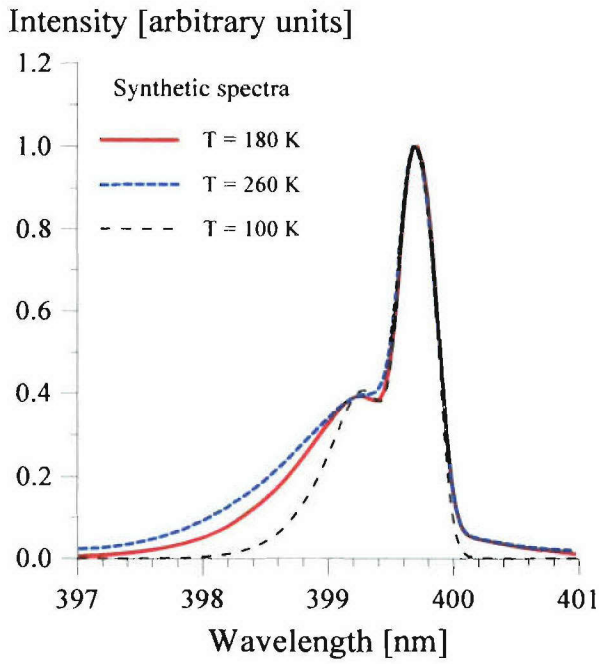

Figure 7. $N_2(C^3\Pi_u \rightarrow B^3\Pi_g)$ synthetic spectra (1→4 band) at T=100, 180, and 160 K, illustrating the temperature inference method sensitivity.

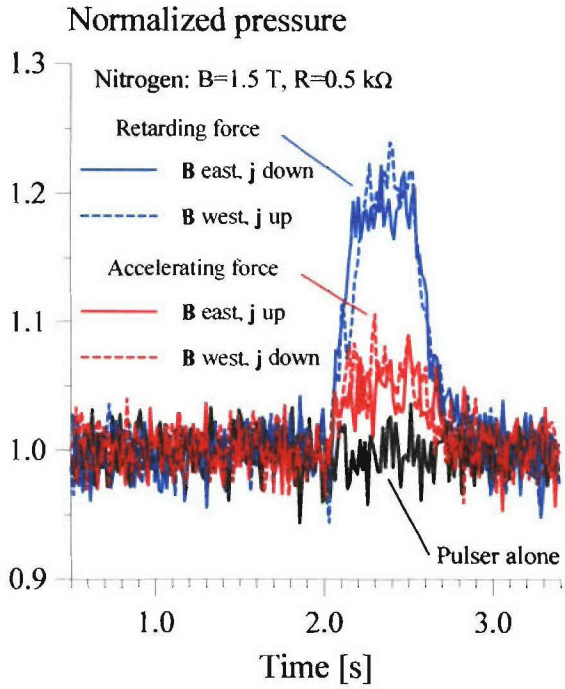

Figure 8. Normalized static pressure traces at the conditions of Figs. 3-5. Lorentz force is applied for 0.5 sec duration. Two pressure traces corresponding to two combinations of current (**j**) and magnetic field (**B**) vectors are shown for both accelerating and retarding force directions.

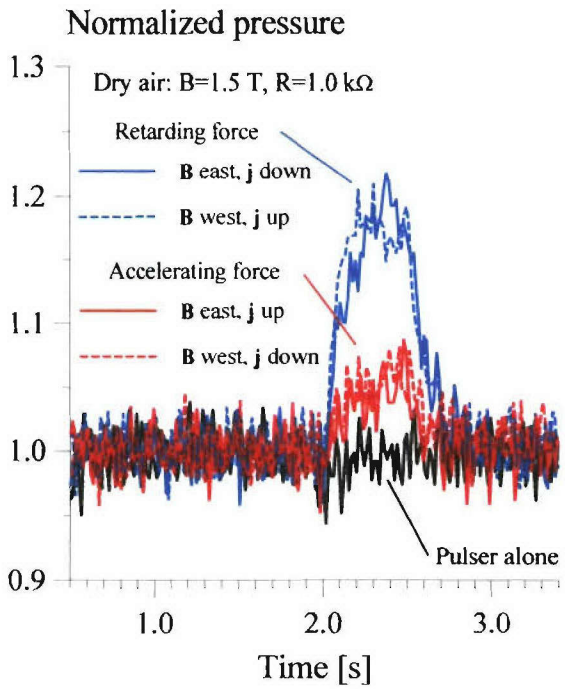

Figure 9. Normalized static pressure traces in M=3 dry air flows at P_0=250 torr, P_{test}=8.7 torr, B=1.5 T, ν=40 kHz. U_{PS}=2 kV, R=1.0 kΩ. Lorentz force is applied for 0.5 sec duration. The legend is the same as in Fig. 6.

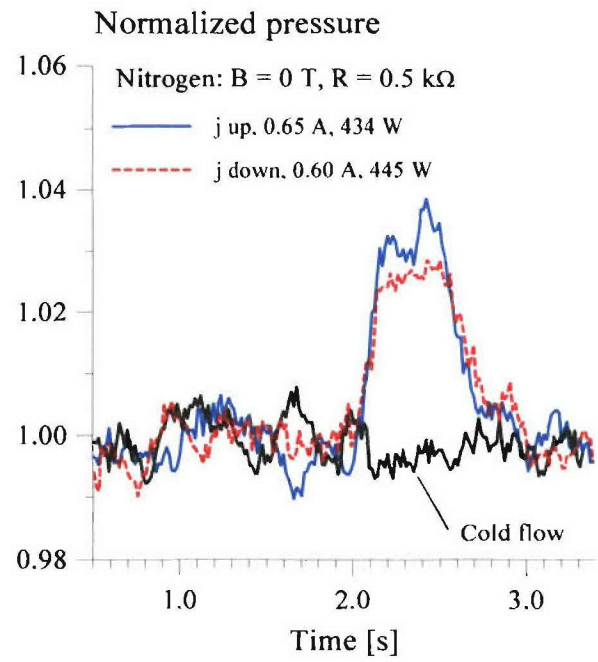

Figure 10. Normalized static pressure traces in M=3 nitrogen flows at P_0=250 torr. U_{PS}=1 kV, R=0.5 kΩ, without magnetic field. Two pressure traces corresponding to two different transverse DC electric field polarities are shown.

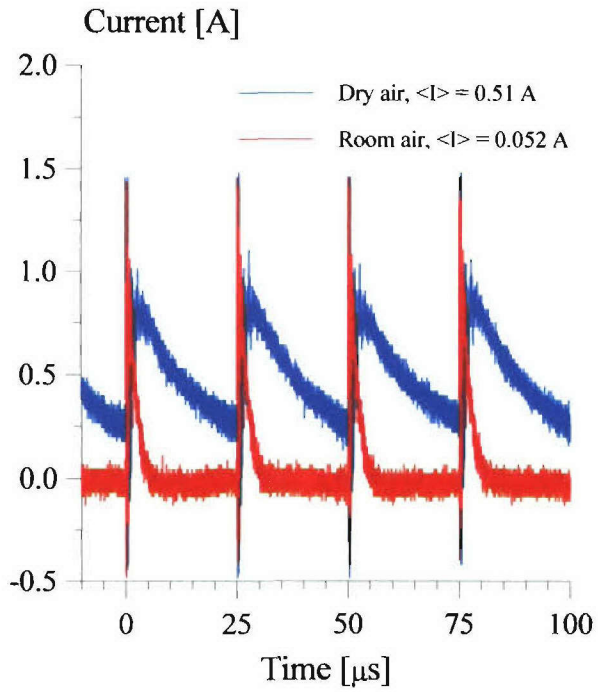

Figure 11. Sustainer (Faraday) current traces in dry air and in room air, at the conditions of Fig. 7. U_{PS}=2 kV, R=1.0 kΩ. Time-averaged currents are 0.51 A (dry air) and 0.052 A (room air).

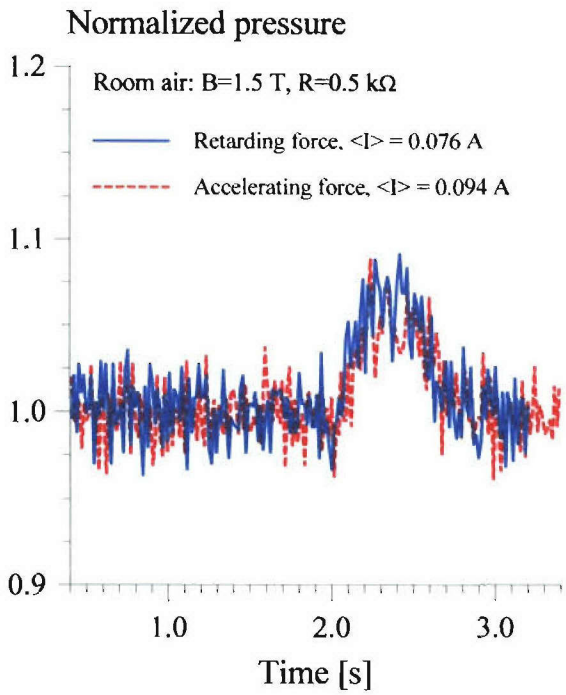

Figure 12. Normalized static pressure traces in M=3 room air flows at the conditions of Fig. 8. Lorentz force is applied for 0.5 sec duration.

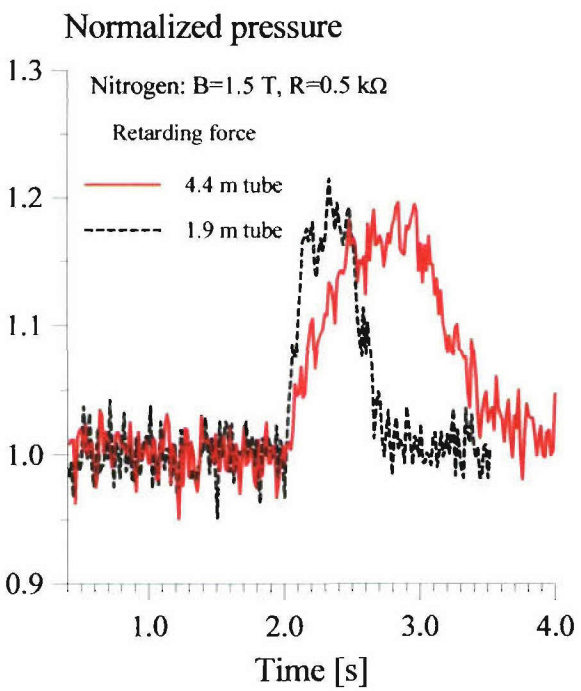

Figure 13. Effect of the pressure tap line length on the measured static pressure rise/fall time. Retarding Lorentz force is applied for 0.5 sec duration. Nitrogen flow conditions are the same as in Figs. 4, 6.

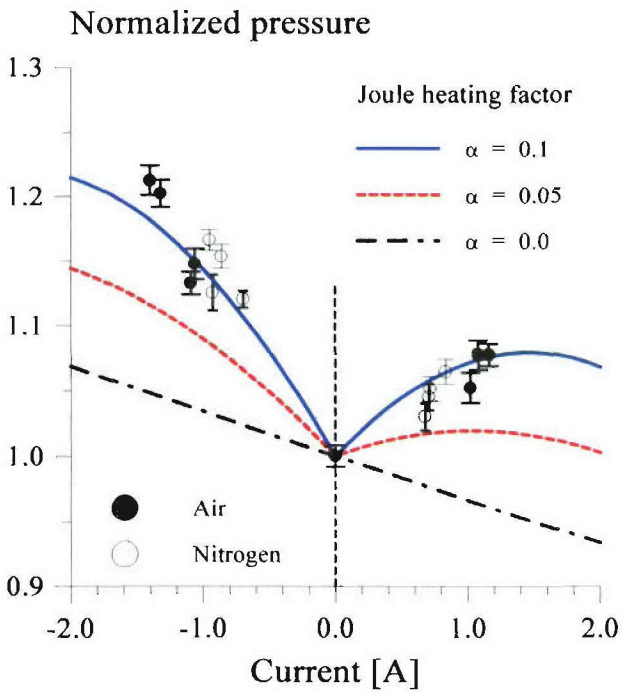

Figure 14. Experimental and calculated normalized pressure in nitrogen and air at P_0=250 torr, U_{PS}=1 kV, and R=0.5 kΩ Calculation results are shown for different values of the Joule heating factor, α.

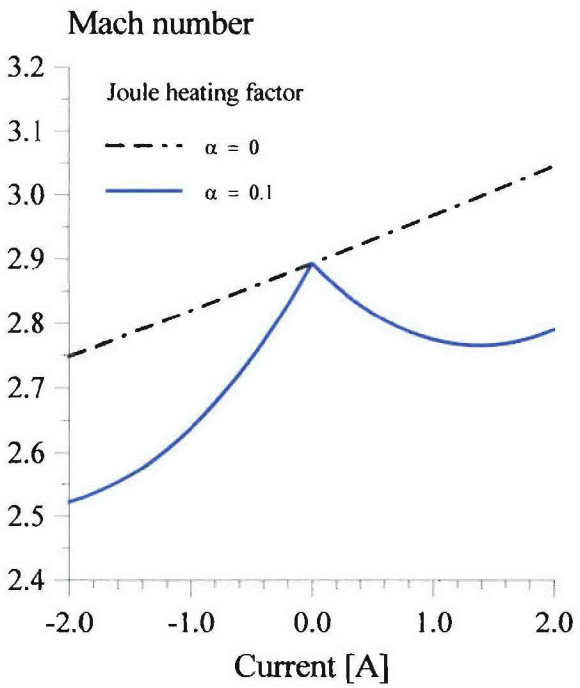

Figure 15. Calculated Mach number change in nitrogen and air at P_0=250 torr, for α=0.1. At I=±1 A, the Mach number change is 0.13 (from M=2.64 to M=2.77).

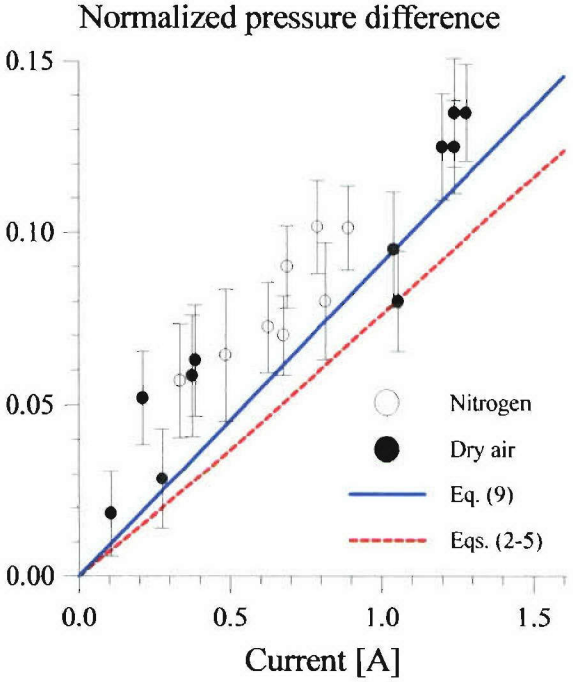

Figure 16. Experimental and calculated normalized pressure difference, $(\Delta p_R - \Delta p_A)/p$, as a function of the MHD current.

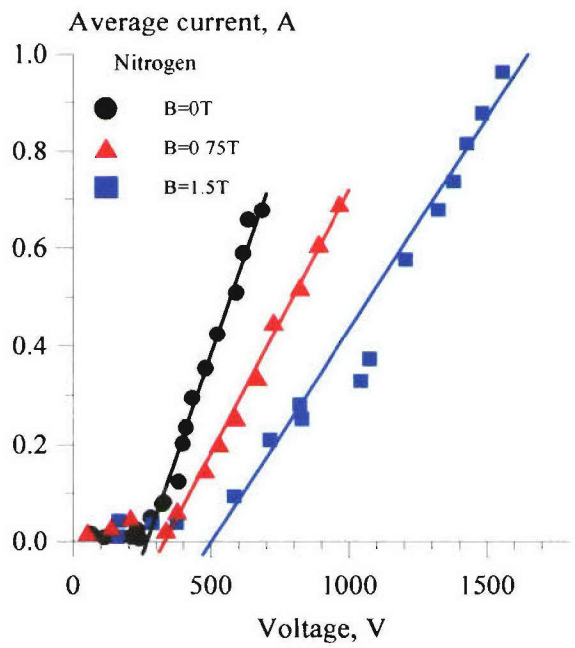

Figure 17. Current voltage characteristics of the sustainer discharge in M=3 flows of nitrogen at different values of magnetic field. P_0=250 torr, P_{test}=7.5 torr, v=40 kHz.

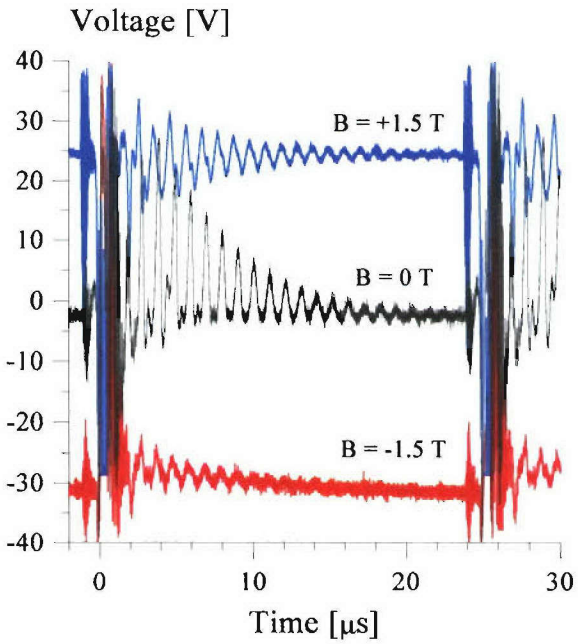

Figure 18. MHD open voltages in M=3 nitrogen flows at different values of magnetic field. P_0=250 torr, P_{test}=7.5 torr, v=40 kHz.

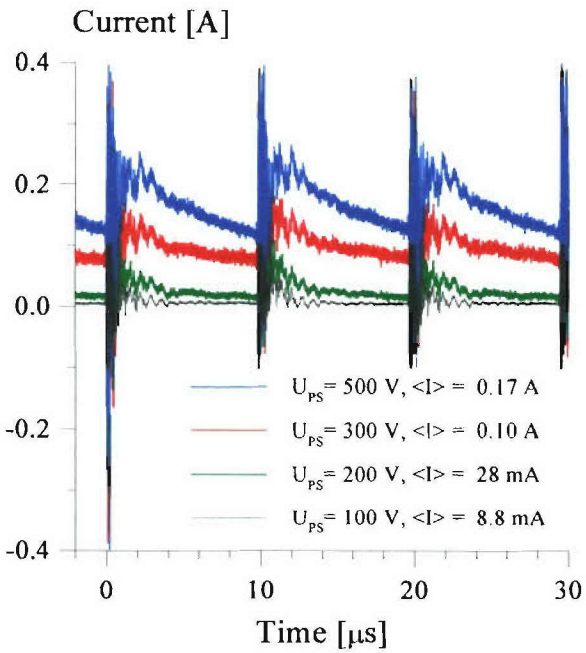

Figure 19. Sustainer current vs. sustainer voltage in M=3 nitrogen flows. P_0=250 torr, ν=100 kHz, load resistance 500 Ω.

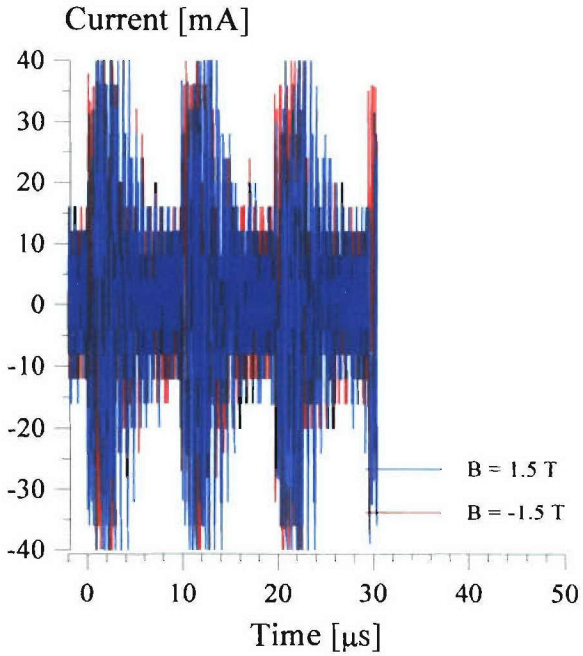

Figure 20. MHD currents in M=3 nitrogen flows. P_0=250 torr, ν=100 kHz, load resistance 500 Ω. No DC voltage is applied to the electrodes.

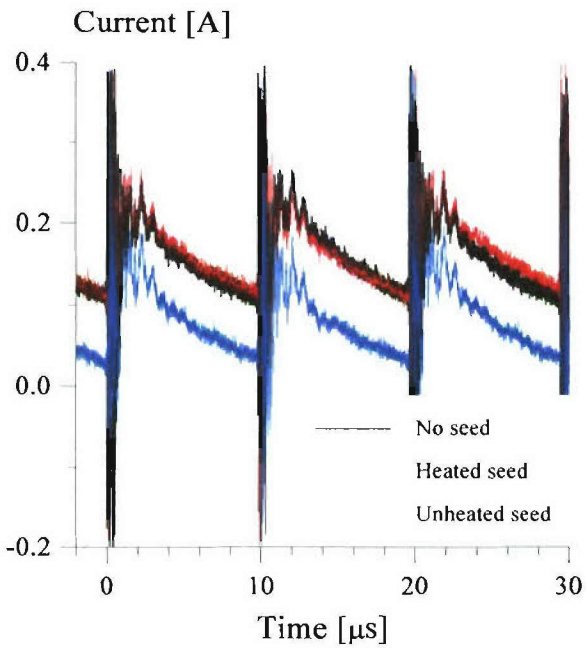

Figure 21. Sustainer currents in M=3 nitrogen flows seeded with cyclopentene. P_0=250 torr, ν=100 kHz, U_{PS}=500 V, load resistance 500 Ω.

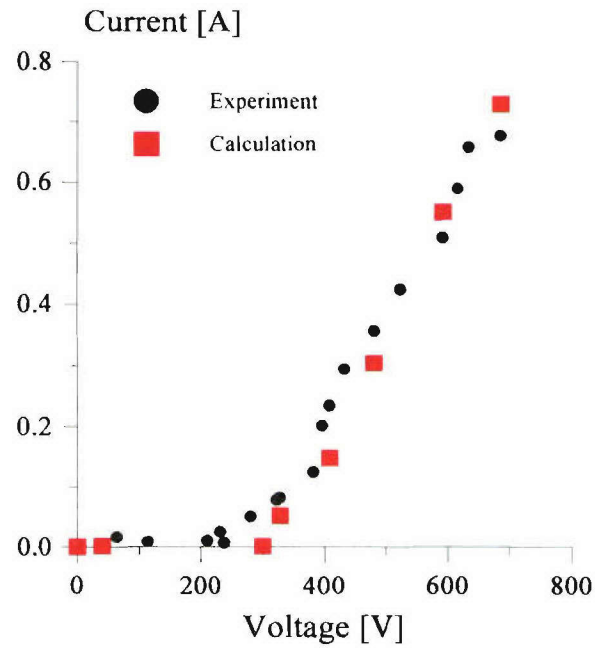

Figure 22. Experimental and calculated current voltage characteristics of the sustainer discharge in nitrogen.

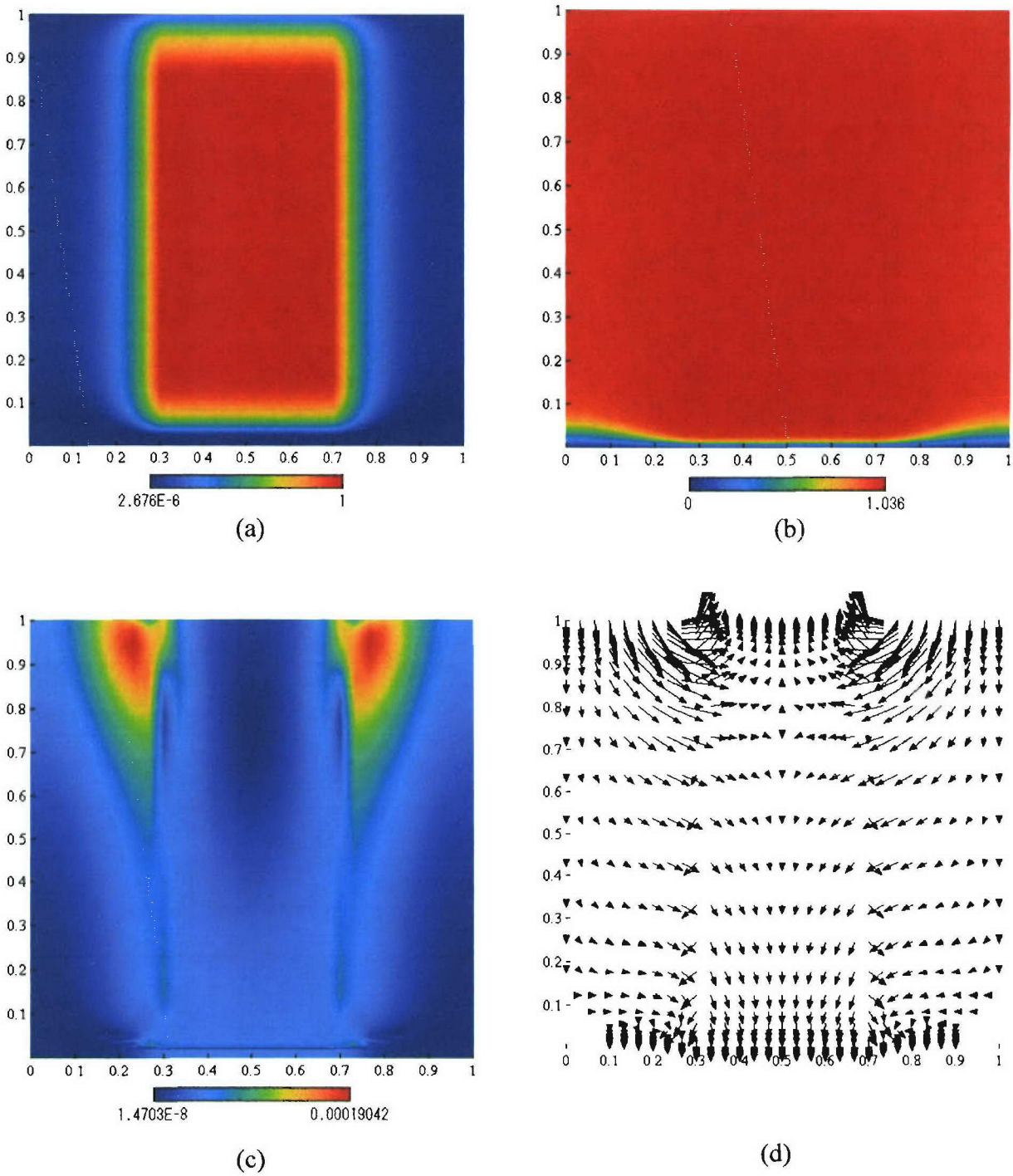

Figure 23. Electron density distribution (a), potential distribution (b), current distribution (c), and current vector field (d) in a non-self-sustained DC discharge with no B field applied. U=50 V, maximum electron density $n_e=2\cdot10^{11}$ cm^3/sec (electrical conductivity of 0.074 mho/m), secondary emission coefficient $\gamma=1.0$. Discharge current is 0.52 mA.

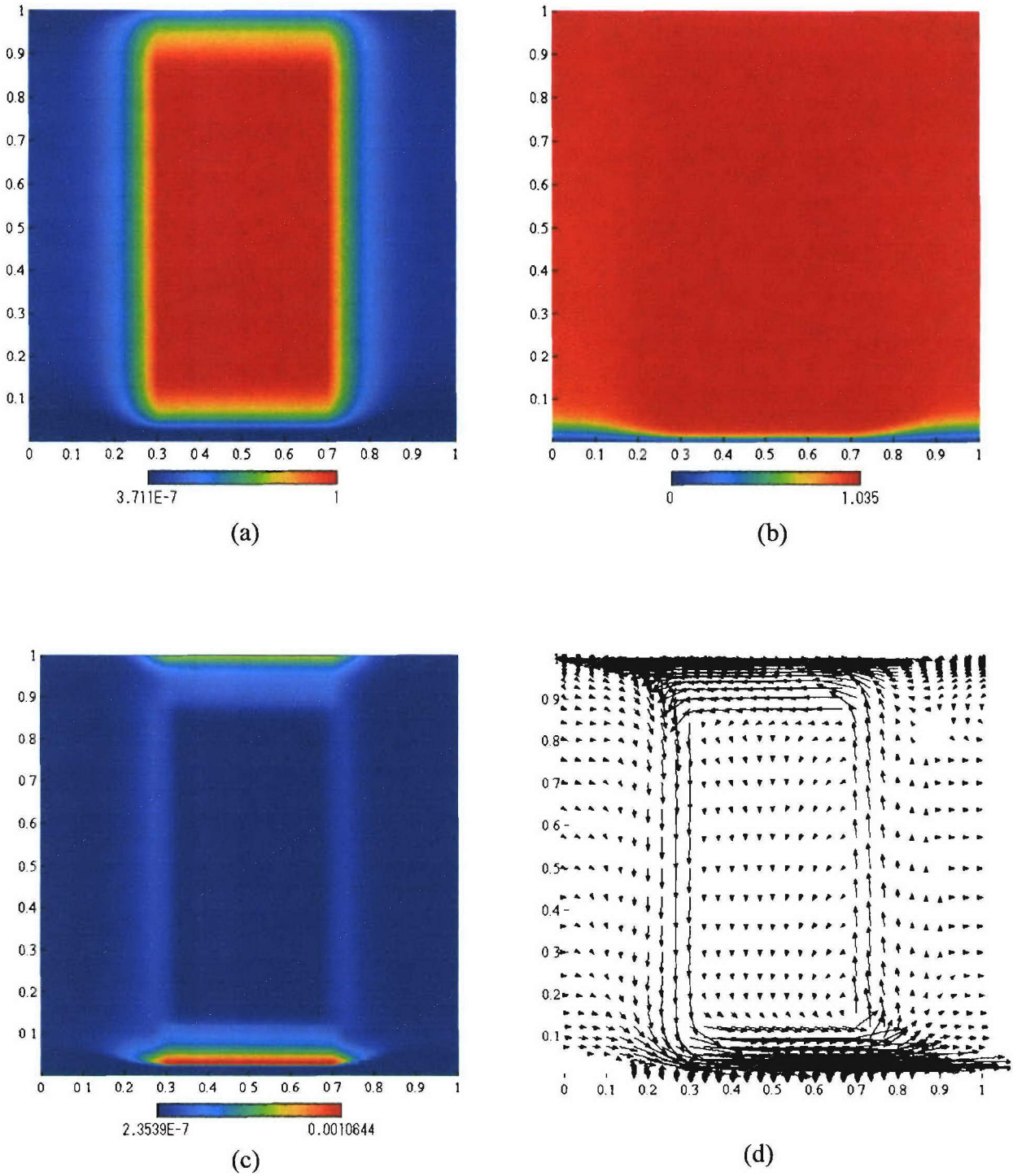

Figure 24. Electron density distribution (a), potential distribution (b), current distribution (c), and current vector field (d) in a non-self-sustained DC discharge at B_z=1.5 T. U=50 V, maximum electron density $n_e=2\cdot10^{11}$ cm^3/sec (electrical conductivity of 0.074 mho/m), secondary emission coefficient γ=1.0. Discharge current is 0.26 mA.